



HAL
open science

Amphiphilic phosphorous dendron micelles co-deliver microRNA inhibitor and doxorubicin for augmented triple negative breast cancer therapy

Liang Chen, Mengsi Zhan, Jin Li, Liu Cao, Huxiao Sun, Régis Laurent, Serge Mignani, Anne- Marie Caminade, Jean-Pierre Majoral, Xiangyang Shi

► To cite this version:

Liang Chen, Mengsi Zhan, Jin Li, Liu Cao, Huxiao Sun, et al.. Amphiphilic phosphorous dendron micelles co-deliver microRNA inhibitor and doxorubicin for augmented triple negative breast cancer therapy. *Journal of materials chemistry B*, 2023, 11 (24), pp.5483-5493. 10.1039/D2TB02114E . hal-04144460

HAL Id: hal-04144460

<https://hal.science/hal-04144460>

Submitted on 28 Jun 2023

HAL is a multi-disciplinary open access archive for the deposit and dissemination of scientific research documents, whether they are published or not. The documents may come from teaching and research institutions in France or abroad, or from public or private research centers.

L'archive ouverte pluridisciplinaire **HAL**, est destinée au dépôt et à la diffusion de documents scientifiques de niveau recherche, publiés ou non, émanant des établissements d'enseignement et de recherche français ou étrangers, des laboratoires publics ou privés.

ARTICLE

Amphiphilic phosphorous dendron micelles co-deliver microRNA inhibitor and doxorubicin for augmented triple negative breast cancer therapy

Received 00th January 20xx,
Accepted 00th January 20xx

DOI: 10.1039/x0xx00000x

Liang Chen^{a,b,c}, Mengsi Zhan^a, Jin Li^a, Liu Cao^a, Huxiao Sun^a, Régis Laurent^{b,c}, Serge Mignani^{d,e}, Anne-Marie Caminade^{b,c*}, Jean-Pierre Majoral^{b,c*}, Xiangyang Shi^{a,e*}

Abstract: Combined chemo/gene therapy of cancer through different action mechanisms has been emerging to enhance the therapeutic efficacy of cancer, and still remains to be a challenging task due to the lack of highly effective and biocompatible nanocarriers. In this work, we report a new nanosystem based on amphiphilic phosphorus dendron (1-C12G1) micelles to co-deliver microRNA-21 inhibitor (miR-21i) and doxorubicin (DOX) for combination therapy of triple negative breast cancer. The amphiphilic phosphorus dendron bearing a long linear alkyl chain and ten protonated pyrrolidine surface groups was prepared and was demonstrated to form micelles in water solution and have a hydrodynamic size of 103.2 nm. The micelles are shown to be stable, enable encapsulation of an anticancer drug DOX with optimal loading content (80%) and encapsulation efficiency (98%), and can compress miR-21i to form polyplexes to render it with good stability against degradation. The co-delivery system of 1-C12G1@DOX/miR-21i polyplexes has a pH-dependent DOX release profile, and can be readily phagocytosed by cancer cells to inhibit them due to the different anticancer mechanisms, which was further validated after intravenous injection to treat an orthotopic triple-negative breast tumor model in vivo. With the proven biocompatibility under the studied doses, the developed amphiphilic phosphorus dendron micelles could be developed as an effective nanomedicine formulation for synergistic cancer therapy.

10th Anniversary Statement

On the occasion to celebrate the 10th anniversary of Journal of Materials Chemistry B (JMCB), I have witnessed the continuous growth the journal, a leading Royal Society of Chemistry (RSC) journal publishing papers in the fields of all aspects of biomaterials research. Until now, our group has published 31 papers in JMCB in the area of drug/gene delivery, molecular imaging, biosensing, and tumor therapy/theranostics. I have also been an active reviewer for JMCB, and was awarded as an excellent reviewer for JMCB in 2020 by the RSC. During my experience with JMCB, my team members and collaborators, as well as my colleagues working in the field of biomaterials all feel that JMCB is an excellent journal and forum to publish biomaterials-related research work in terms of its processes of peer review, editorial work, production, and distribution.

Introduction

Although considerable progresses have been made in the early diagnosis and treatment, multidrug resistance and side-effect of traditional chemotherapeutics are still major bottle-neck problems to be solved for effective cancer therapy. Therefore, various strategies have been developed to overcome these problems. Among them, the combined drug/gene co-delivery strategy has been paid much attention to enhance the efficacy of cancer therapy through the induced synergy exerted by each drug with its inherent mechanistic action.¹⁻³

MicroRNAs (miRNAs) are known to be a family of small, endogenous noncoding RNAs that can post-transcriptionally regulate the translation and stability of mRNAs.^{4,5} The disorder of miRNAs has been disclosed in a variety of cancer types and is considered as a sign of cancer.⁶ Importantly, due to the complexity of cancer-associated signal networks, the multiple targeting capability of tumor suppression miRNAs has attracted extensive attention in improving the cancer therapy efficacy.⁶ In this context, anti-cancer therapies based on miRNA have been developed either alone or together with chemical drugs, aiming to improve the therapeutic efficacy.⁷ In particular, microRNA-21 (miR-21) has been noticed to be highly expressed in triple negative breast cancer (TNBC), pancreatic cancer, or other types of cancer.^{8,9} The high expression of miR-21 is found to promote tumor growth and proliferation by acting on the phosphatase and TENSin homolog (PTEN)-associated pathways.⁸⁻¹⁰

^a State Key Laboratory for Modification of Chemical Fibers and Polymer Materials, Shanghai Engineering Research Center of Nano-biomaterials and Regenerative Medicine, College of Biological Science and Medical Engineering, Donghua University, Shanghai 201620, People's Republic of China. E-mail: xshi@dhu.edu.cn

^b Laboratoire de Chimie de Coordination du CNRS, 205 Route de Narbonne, BP 44099, 31077 Toulouse CEDEX 4, France. E-mail: anne-marie.caminade@lcc-toulouse.fr (A.M.C.) and jean-pierre.majoral@lcc-toulouse.fr (J.P.M.)

^c Université de Toulouse, UPS, INPT, 31077 Toulouse CEDEX 4, France

^d Université Paris Descartes, PRES Sorbonne Paris Cité, CNRS UMR 860, Laboratoire de Chimie et de Biochimie Pharmacologiques et Toxicologique, 45, rue des Saints Pères, 75006 Paris, France

^e CQM - Centro de Química da Madeira, Universidade da Madeira, Campus da Penteada, 9020-105 Funchal, Portugal

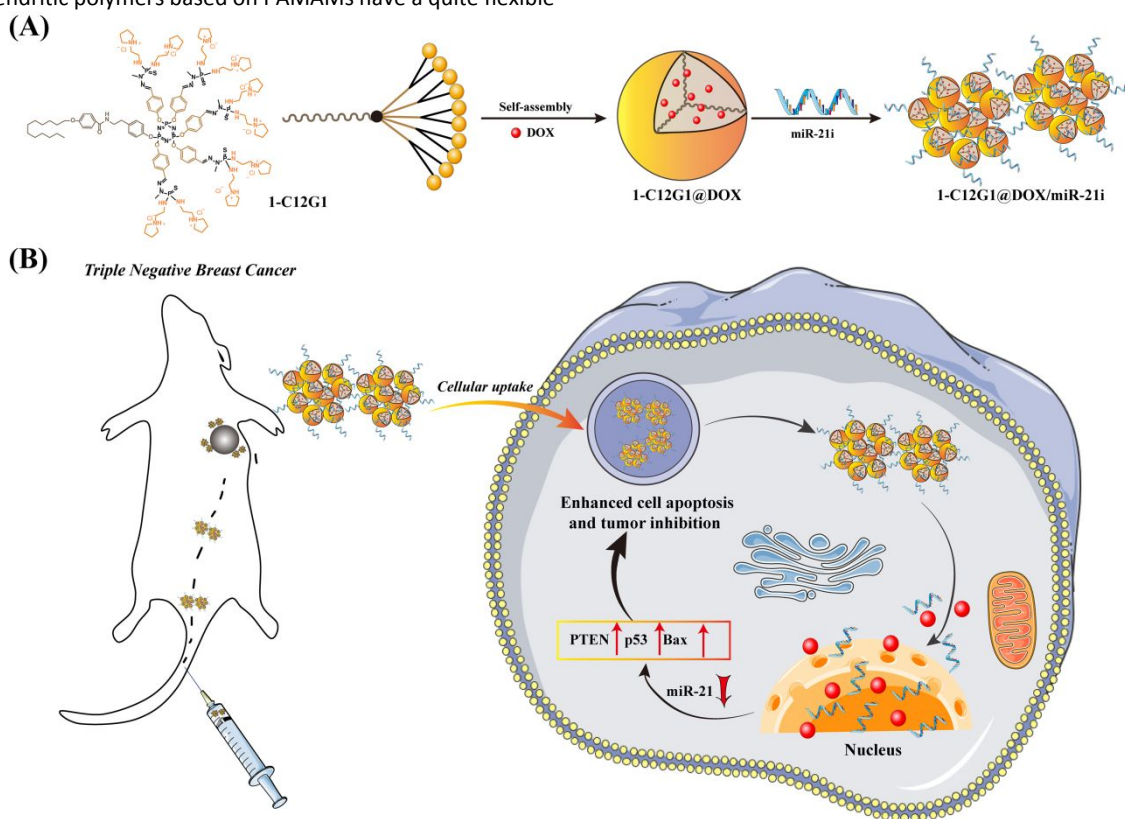
Electronic Supplementary Information (ESI) available: [details of any supplementary information available should be included here]. See DOI: 10.1039/x0xx00000x

A recent study showed that knocking down of miR-21 has marginal impact on the cancer cell viability, but the inhibition of cell growth was improved when the cancer cells were treated with an additional anticancer drug. This suggests that the chemotherapy effect of cancer cells can be sensitized through inhibition of miR-21.¹⁰ Previously, we have shown that generation 5 poly(amidoamine) (PAMAM) dendrimer-entrapped gold nanoparticles (NPs) can be utilized as a carrier to co-deliver anticancer drug gemcitabine and miR-21i to pancreatic cancer cells, thus significantly enhancing the therapeutic efficacy of cancer cells in comparison to the single delivery of gemcitabine.¹¹ In another study, hyaluronic acid-chitosan NPs were used to encapsulate microRNA and doxorubicin (DOX) for improved therapy of cancer cells.³ These co-delivery systems are able to encapsulate and controllably deliver different payloads of therapeutics to the site of disease to exert their therapeutic functions in a synergistic fashion.¹⁰⁻¹⁵ For the developed nanomedicine platforms, it is of great importance to effectively load both drug and genetic material with a good morphology control.^{3, 16-19} An ideal carrier system should have a positive surface potential allowing for effective compression of the negatively charged genetic materials, and hydrophobic interior cavities allowing for effective encapsulation of hydrophobic anticancer drugs. Although PAMAM dendrimers⁸ or newly developed core-shell tecto dendrimers¹¹ were demonstrated to have such features, the volume of their internal cavities is quite limited.

In view of the recent developments, amphiphilic dendrimers or dendrons that can form micelles or dendrimerosomes have received a great deal of attention for co-delivery of drugs and genes.^{16, 20, 21} The reported dendritic polymers based on PAMAMs have a quite flexible

molecular structure, which is not ideal for enhanced gene delivery. In a very recent study,²² we have shown that core-shell tecto dendrimers possessing rigid core of phosphorous dendrimers and PAMAM shell dendrimers display much more enhanced gene compression and delivery efficiency than the counterpart having both PAMAM core and shell dendrimers. Very recently, we have shown that amphiphilic phosphorous dendrons with either negatively charged tyramine-bearing two dimethylphosphonate sodium salt²³ or positively charged protonated pyrrolidine moieties²⁴ can be used to encapsulate hydrophobic drugs to fight inflammatory disease or cancer. Therefore, it is quite logic to develop a phosphorous dendron-based micellar system to co-deliver both chemical drug and gene (e.g., miR-21i) for enhanced cancer therapy.

Here, in this present study, we introduced a novel amphiphilic phosphorous dendron material to form micelles. The amphiphilic phosphorus dendron (1-C12G1, Scheme 1A and Figure 1) bearing a long linear alkyl chain (C₁₂H₂₅) and ten protonated pyrrolidine groups on the surface was first synthesized and then assembled to form stable nanomicelles for encapsulation of anticancer drug DOX and complexation of miR-21i. The physicochemical property of the dendrons and dendron micelles, drug release profile, anticancer cytotoxicity, and cellular uptake behavior were systematically investigated, and the co-delivery of DOX and miR-21i for effective cancer therapy was validated using an orthotopic triple-negative breast tumor model (Scheme 1B). According to our literature investigation, this study represents a very first example associated to the use of phosphorous dendron micelles for drug/gene co-delivery to fight cancer.



Scheme 1. (A) Preparation of 1-C12G1@DOX/miR-21i polyplexes. (B) Co-delivery treatment of a tumor model *in vivo*.

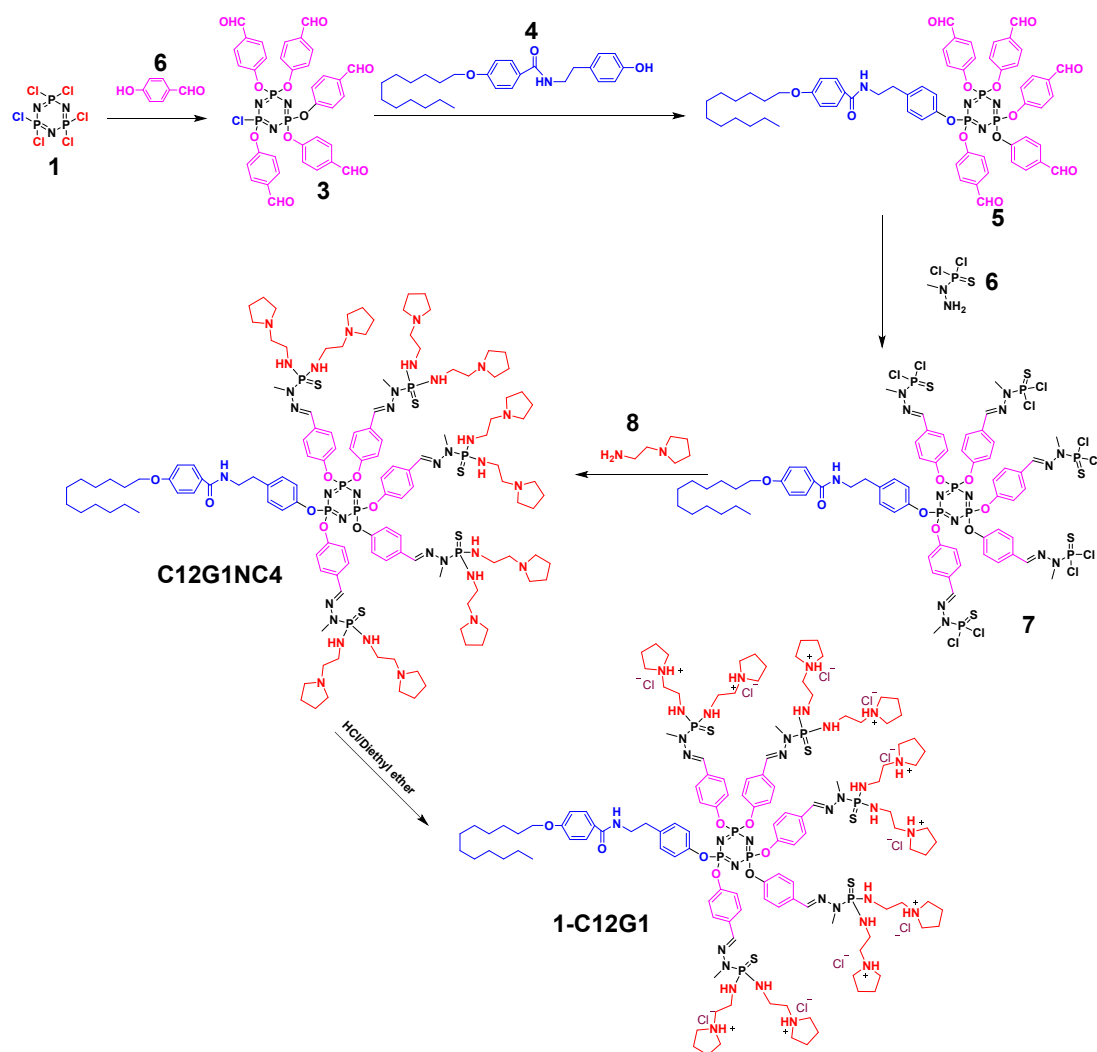


Figure 1. Synthesis of amphiphilic phosphorus dendrons.

Results and discussion

Preparation and characterization of amphiphilic phosphorus dendrons

As illustrated in Figure 1, a new amphiphilic phosphorus dendron with hydrophobic alkyl chain ($C_{12}H_{25}$), rigid structure (benzene ring and double bond) and hydrophilic group (protonated pyrrolidine) was synthesized. This dendron was thoroughly characterized with various NMR techniques (Figures S1-S4). Meanwhile, the 1-C12G1 dendrons were dissolved in water and the ability to form micelles was examined through the critical micelle concentration (CMC) determination (Figure 2A). Clearly, the CMC of the micelles was determined to be $151 \mu\text{M}$. Dynamic light scattering was also employed to determine the hydrodynamic diameter and polydispersity index (PDI) of the micelles. The 1-C12G1 dendron micelles display a hydrodynamic diameter about 103.2 nm (Figure S5A) with a narrow distribution (PDI = 0.798, Table S1). After dilution to a concentration around 5 times lower than the CMC, the hydrodynamic diameter of the micelles does not seem to have any

significant change (99 nm , Figure S5B) and the PDI was even lower (0.314, Table S1). This suggests that the dendron micelles generated by 1-C12G1 display a good colloidal stability. The morphology of the 1-C12G1 micelles was also examined by transmission electron microscopy (TEM), and the 1-C12G1 micelles exhibit a spherical shape with an mean size of 25 nm (Figure S5C).

Preparation and characterization of 1-C12G1@DOX and 1-C12G1@DOX/miR-21i polyplexes

We next loaded the anticancer drug DOX within the micelles to form the 1-C12G1@DOX complexes. The loading content and encapsulation efficiency of the micelles were first investigated by changing the 1-C12G1/DOX molar ratios. As shown in Table 1, at the 1-C12G1@DOX molar ratio of 1: 25, both the loading content and encapsulation efficiency are quite high, reaching 79.2% and 97.9%, respectively. Thus, the 1-C12G1@DOX with the molar ratio of 1: 25 was chosen for following investigations. The high drug-loading capacity may be caused by the molecular structure of 1-C12G1 with rigid hydrophobic branches, generating micelles with large hydrophobic cores for encapsulation of significant amount of drug, similar to the micelles formed from lipids.²⁵

ARTICLE

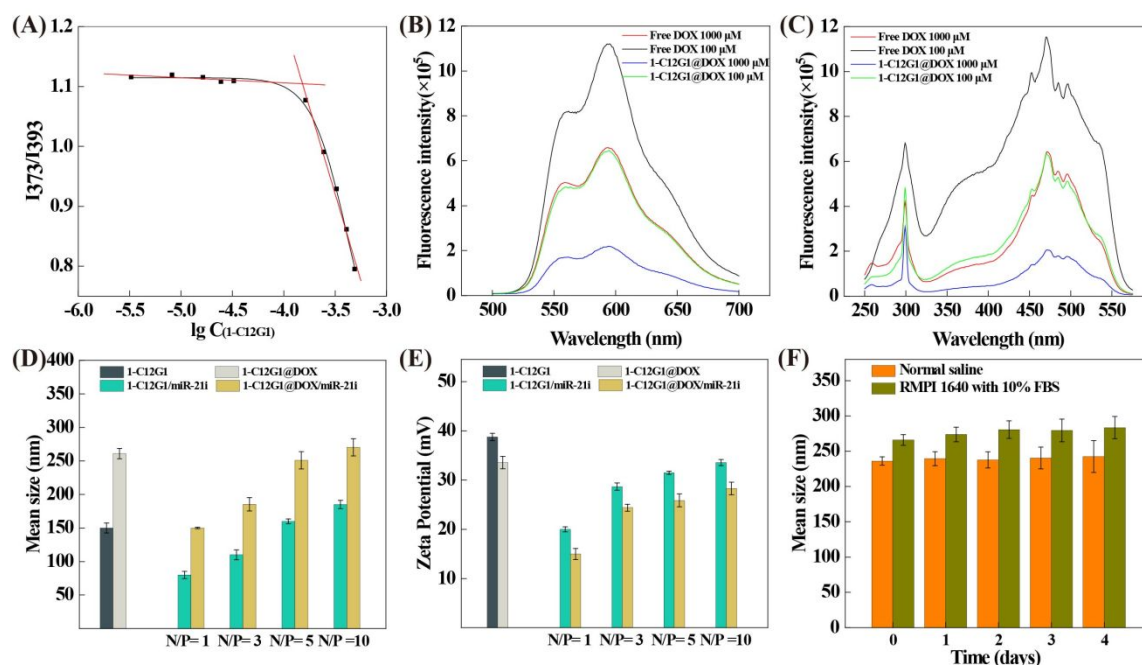


Figure 2. Determination of the CMC of 1-C12G1 micelles using the fluorescent dye pyrene (A). Fluorescence emission (B) and excitation (C) spectra of free DOX and 1-C12G1@DOX. Mean hydrodynamic diameter (D) and zeta potential (E) of 1-C12G1, 1-C12G1@DOX, 1-C12G1/miR-21i and 1-C12G1@DOX/miR-21i. (F) Stability assessments of 1-C12G1@DOX/miR-21i in different aqueous media as assessed by their mean hydrodynamic size changes at 37 °C for different time periods.

Table 1. Optimizing the loading content and encapsulation efficiency of 1-C12G1 micelles.

1-C12G1: DOX mass ratio	Drug encapsulating efficiency (%)	Drug loading content (%)
1: 15	99.81 ± 0.5	69.9 ± 0.4
1: 20	98.11 ± 0.7	75.4 ± 0.5
1: 25	97.94 ± 1.1	79.2 ± 0.8
1: 30	83.60 ± 1.3	82.1 ± 1.0
1: 35	77.17 ± 2.8	78.3 ± 1.5

To further investigate the colloidal stability of 1-C12G1@DOX micelles, the hydrodynamic diameter of 1-C12G1@DOX was checked at different concentrations (Figure S6). At a high DOX concentration, the hydrodynamic diameter of the 1-C12G1@DOX micelles is around 221 nm (PDI = 0.286, Figure S6A and Table S1). After 10 times dilution, the hydrodynamic diameter and PDI of the micelles do not show any appreciable changes (218 nm and 0.290, Figure S6B and Table S1). This means that the drug-loaded micelles also possess good colloidal stability, similar to the drug-free micelles. The morphology of the 1-C12G1@DOX micelles was also observed by TEM (Figure S6C), and the drug-loaded micelles are spherical, similar to the drug-free ones. The larger mean size of the 1-C12G1@DOX micelles (42 nm) than that of the drug-free ones should be due to the DOX loading that

expands the overall geometry of the micelles. The fluorescence properties of free DOX and 1-C12G1@DOX were investigated (Figure 2B-C). Due to fluorescence quenching effect similar to our previous work,²⁴ the free DOX exhibits higher fluorescence intensity than 1-C12G1@DOX at the same DOX concentration. Meanwhile, both free DOX and 1-C12G1@DOX display stronger fluorescence intensity at a low concentration than at a high concentration.

Next, we used 1-C12G1@DOX micelles to compact miR-21i to form 1-C12G1@DOX/miR-21i polyplexes. Gel retardation assay data shown in Figure S7A reveal that the miR-21i can be fully compacted by the 1-C12G1@DOX micelles at an N/P ratio of 1: 1 or above. Then, we examined the stability of 1-C12G1@DOX/miR-21i polyplexes (N/P value = 5: 1) exposed to normal saline (NS) at 37 °C (Figure S7B). Clearly, the miR-21i complexed with 1-C12G1@DOX micelles can be protected from degradation for up to 12 h and 24 h. In contrast, naked miR-21i is not stable and can be degraded to have diminished bands under the same conditions.

The hydrodynamic size and surface potential of the polyplexes were key factors to assess the performance of gene cargos.²⁶ We then examined the zeta potential and mean hydrodynamic diameter of the polyplexes. As shown in Figure 2D-E, with the increase of N/P ratio, the compaction interaction between 1-C12G1@DOX and miR-21i can be saturated to lead to insignificant changes of the surface potential of the polyplexes as the surface of the polyplexes is fully covered with the positively charged dendrons. Meanwhile, more

dendrons contribute to the compression of miR-21i to cause the size decrease of the polyplexes until reaching the point of saturation. According to the literature,²⁷ vector/gene polyplexes with a positive surface potential and a size of around 200 nm are suitable for gene delivery purpose. Therefore, we selected an N/P ratio of 5: 1 to prepare the polyplexes for later experimental investigations.

To evaluate the stability of the 1-C12G1@DOX/miR-21i polyplexes, their hydrodynamic size in both NS and complete cell culture medium at 37 °C was examined for different time periods (Figure 2F). No obvious aggregation of polyplexes were observed and the polyplexes show approximately similar sizes ranging from 225 to 270 nm for 4 days. This indicates that the 1-C12G1@DOX/miR-21i polyplexes display desired stability, which is ready for further studies. Meanwhile, the 1-C12G1@DOX/miR-21i polyplexes have similar hydrodynamic diameter and PDI at different concentrations (Figure S8 and Table S1), reflecting their good colloidal stability. Interestingly, the 1-C12G1@DOX/miR-21i polyplexes exhibit a smaller mean size (36 nm, Figure S8C) than the 1-C12G1@DOX (42 nm) before miR-21i complexation, which may be caused by the compaction of the micelles after electrostatic interaction with the miR-21i.

For an ideal drug delivery system employed in cancer therapy, it is crucial to have the therapeutic agent to be controllably released at the tumor site, thus avoiding the non-desired toxicity to normal tissues. Since the tumor lesion is generally slightly acidic in pH, acid-triggered fast drug release at tumor site is undoubtedly beneficial to improve the cancer therapy performance.^{28, 29} Next, the release profile of DOX from the 1-C12G1@DOX/miR-21i was investigated at 37 °C and in phosphate buffer at both pH 5.5 and pH 7.4 (Figure S9). DOX release from the polyplexes can reach around 51% and 30% within the first 10 h at pH 5.5 and pH 7.4, respectively, after which continuous slow release of DOX remains. At the same time point, the DOX release at pH 5.5 is faster than at pH 7.4, likely owing to the protonation of DOX at a lower pH to lead to increased water solubility of DOX, in agreement with the literature.³⁰

Enhanced therapy of cancer cells *in vitro*

Previous studies have shown that miRNAs have synergistic antitumor effects in combination with conventional chemotherapy.^{3, 31, 32} Hence, we evaluated the antiproliferation efficiency of the developed 1-C12G1@DOX/miR-21i polyplexes using two cell lines, including normal NIH-3T3 cells and MDA-MB-231 cells. As can be seen in Figure 3A, the antiproliferation effect of free DOX towards normal NIH-3T3 cells is higher than that of 1-C12G1@DOX and 1-C12G1@DOX/miR-21i polyplexes at the same DOX concentrations, presumably due to the fact that the sustained DOX release from the micelles leads to a lower DOX concentration for cell treatment. Meanwhile, the viability of NIH-3T3 cells incubated with 1-C12G1 or 1-C12G1/miR-21i does not seem to have any significant changes. As shown in Figure 3B, for cancer cells, no apparent cell death can be observed in the 1-C12G1-treated cells, implying the good cytocompatibility of drug-free 1-C12G1 dendron micelles. The MDA-MB-231 cells treated with 1-C12G1/miR-21i show a reduced cell viability with the increase of equivalent DOX concentration,

suggesting that the delivery of miR-21i to cells may trigger the apoptosis of MDA-MB-231 cells. Free DOX, 1-C12G1@DOX and 1-C12G1@DOX/miR-21i all exhibit remarkable cytotoxicity to MDA-MB-231 cells in a DOX concentration-dependent fashion. Free DOX displays slightly higher cytotoxicity than the 1-C12G1@DOX micelles, but lower cytotoxicity than the 1-C12G1@DOX/miR-21i polyplexes under the identical DOX doses. This suggests that the 1-C12G1@DOX/miR-21i polyplexes can fully utilize the active gradients of both DOX and miR-21i to have a synergistic therapy effect through combination of different mechanisms. The IC₅₀ values of the different formulations are shown in Figure S10, and the anticancer efficiency can be ranked in an order of 1-C12G1@DOX/miR-21i (0.073 μM) > free DOX (0.37 μM) > 1-C12G1@DOX (0.85 μM). The IC₅₀ of 1-C12G1@DOX/miR-21i is approximately 5 times lower than that of free DOX, demonstrating the excellent synergistic therapy effect by integration of both DOX and miR-21i within one micellar formulation.

The intracellular uptake was qualitatively monitored by confocal and fluorescence microscopies (Figure 4). Clearly, after the cells were incubated for 4 h with free DOX, 1-C12G1@DOX and 1-C12G1@DOX/miR-21i, significant fluorescent signals of DOX (red) are shown in the cytoplasm. The overlapped blue (nucleus), red and green (β-actin) fluorescence images show that the red fluorescence associated to DOX is partly colocalized within the cytoplasm and the cell nuclei, suggesting that either free DOX or DOX within the micelles can be internalized firstly within the cytoplasm and then go into the cell nuclei. Similar results can also be obtained through fluorescence microscopic imaging (Figure S11).

The cellular uptake of free DOX, 1-C12G1@DOX and 1-C12G1@DOX/miR-21i by MDA-MB-231 cells were further confirmed by flow cytometry (Figure 3C and Figure S12). These results imply that the MDA-MB-231 cells can be effectively delivered with DOX by the 1-C12G1-based micelles, in agreement with the above confocal and fluorescence microscopic imaging data. Collectively, our results suggest that the 1-C12G1@DOX/miR-21i polyplexes can be successfully taken up by MDA-MB-231 cells, which is amenable to exert their therapeutic activity.

To further investigate if there are synergistic effects of miR-21i and DOX in cell apoptosis, MDA-MB-231 cells were treated with free DOX, 1-C12G1@DOX or 1-C12G1@DOX/miR-21i and analyzed by flow cytometry (Figure 3D and Figure S13). No obvious cell apoptosis can be seen in the group of drug-free 1-C12G1 micelles, similar to the PBS control group. Our results suggest that the 1-C12G1 micelles have a good cytocompatibility in the concentration range investigated. However, cells treated with the 1-C12G1/miR-21i have an apoptosis percentage of 7.06% ± 0.24%, which is significantly higher than the PBS control group (4.21% ± 0.29%, *p* < 0.001), implying the gene therapy efficacy of the miR-21i. Additionally, all of the other three DOX-containing groups exhibit obvious cell apoptosis effect compared to the control group. Similar to our expectation, the cell apoptosis percentage of the 1-C12G1@DOX/miR-21i group (10.5 ± 0.2%) is higher than that of the free DOX (6.1 ± 0.2%, *p* < 0.001) and 1-C12G1@DOX (9.47% ± 0.07%, *p* < 0.05) groups. The obtained data confirmed the synergistic chemo/gene therapeutic efficacy of such a co-delivery system.

ARTICLE

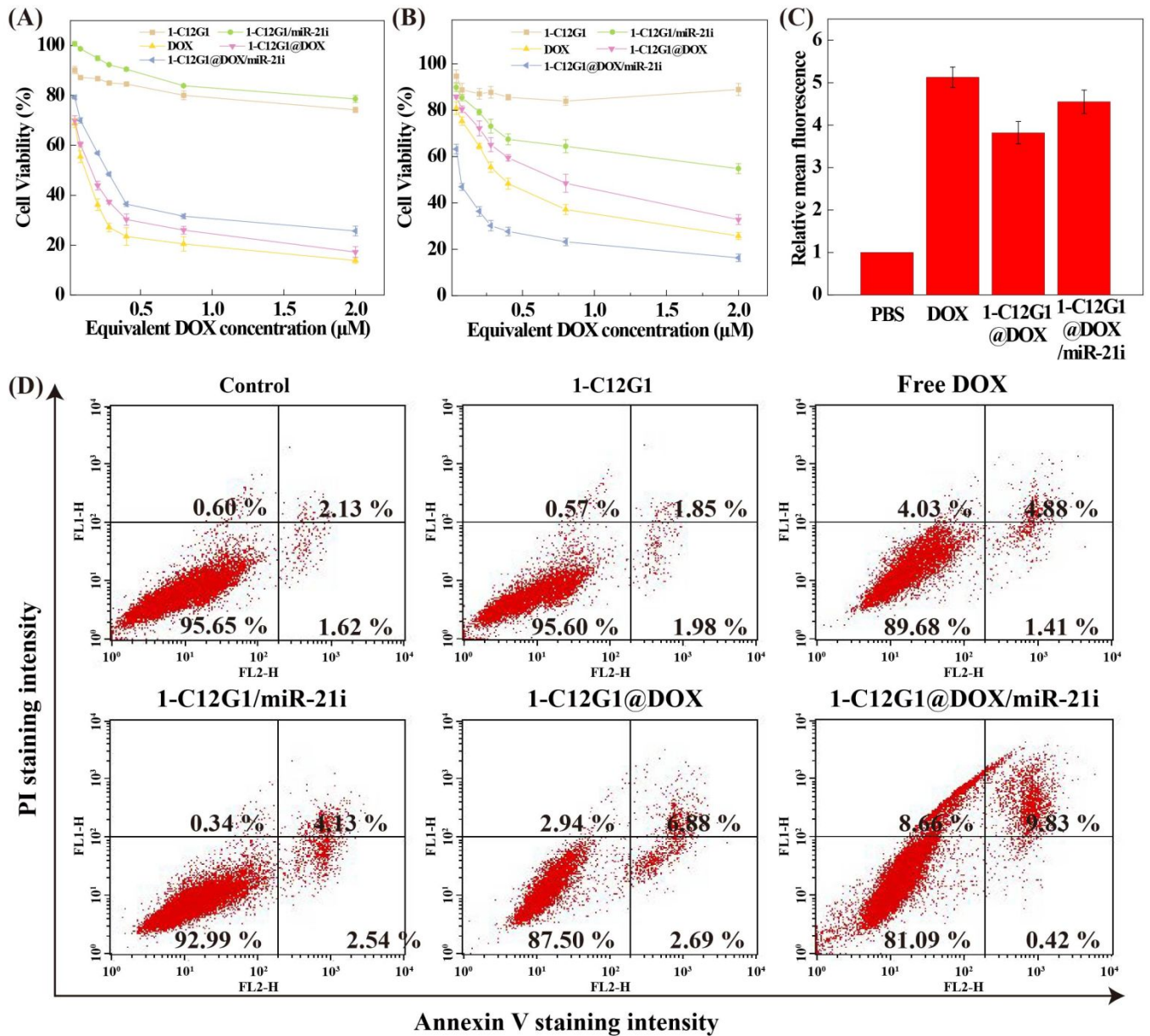


Figure 3. Concentration-dependent cell viability of NIH-3T3 (A) and MDA-MB-231 (B) cells treated with 1-C12G1, 1-C12G1/miR-21i, 1-C12G1@DOX or 1-C12G1@DOX/miR-21i assessed by CCK-8 assay. Data were shown as mean \pm SD (n = 6). (C) Relative mean fluorescence intensity of MDA-MB-231 cells incubated with free DOX, 1-C12G1@DOX or 1-C12G1@DOX/miR-21i (the equivalent concentration of DOX was 1 μM) assayed by flow cytometry. (D) Apoptosis of MDA-MB-231 cells incubated with 1-C12G1, free DOX, 1-C12G1/miR-21i, 1-C12G1@DOX or 1-C12G1@DOX/miR-21i (the equivalent DOX concentration was 1 μM) as assayed by flow cytometry. Phosphate buffered saline (PBS) was utilized as control.

ARTICLE

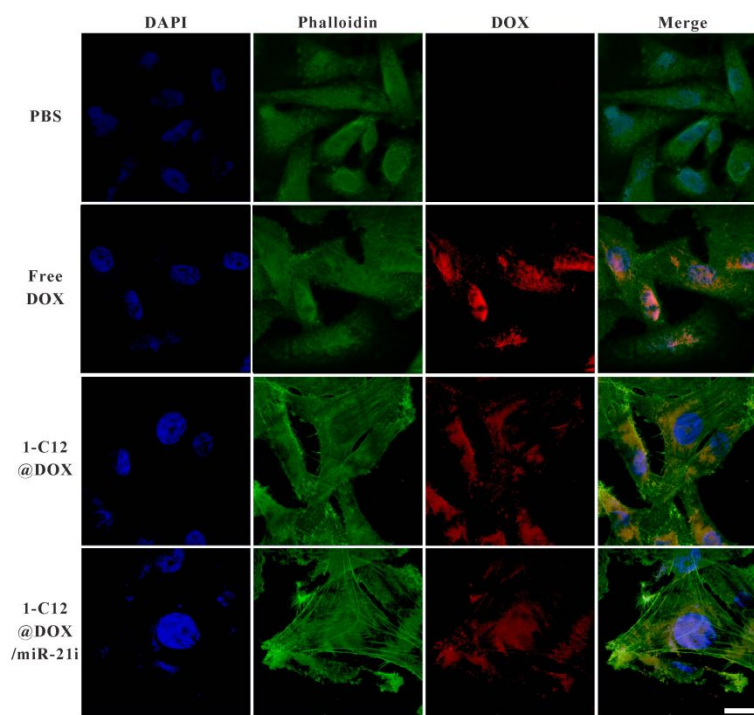


Figure 4. Laser confocal microscopic images of MDA-MB-231 cells treated with free DOX, 1-C12G1@DOX or 1-C12G1@DOX/miR-21i for 4 h (the equivalent DOX concentration was 1 μ M). Scale bar in each panel represents 200 μ m.

The cell apoptosis-associated proteins were examined through Western blotting *in vitro* to further elucidate the molecular mechanism of the cell apoptosis (Figure 5). Significantly increased expression of BAX, p53 and PTEN is observed in cells incubated with free DOX, 1-C12G1/miR-21i, 1-C12G1@DOX and 1-C12G1@DOX/miR-21i. Apparently, in the presence of either miR-21i or DOX, the apoptosis of MDA-MB-231 cells can be promoted. Moreover, the expression levels of all apoptosis-related proteins are the highest in the group of 1-C12G1@DOX/miR-21i among all groups ($p < 0.05$). These results confirm the synergistic chemo/gene therapeutic efficacy of such a co-delivery system, in agreement with the apoptosis assay results obtained by flow cytometry.

Co-delivery treatment of a tumor model *in vivo*

Next, an orthotopic model of TNBC was built to assess the synergistic therapeutic efficacy of 1-C12G1@DOX/miR-21i polyplexes *in vivo* (Figure 6A and Figure S14). Administration of free DOX, 1-C12G1/miR-21i, 1-C12G1@DOX or 1-C12G1@DOX/miR-21i polyplexes leads to great tumor growth inhibition. In contrast, the drug-free 1-C12G1 group does not seem to have any inhibition effect, similar to the NS control group. During the entire treatment period, mice in the NS, 1-C12G1, 1-C12G1/miR-21i, 1-C12G1@DOX or 1-C12G1@DOX/miR-21i treatment groups behave normally, and the

mouse body weight in these different groups has no significant changes (Figure 6B). This implies that the developed 1-C12G1 micelles and the associated polyplexes have no appreciable *in vivo* toxicity during the experimental investigation period. To be opposed, mice treated with free DOX display apparent weight loss. Two mice treated with the free DOX are dead during the treatment period (Figure 6C), while is in contrast to all other groups within 15 days. This should be due to the free DOX-induced high toxicity.³³⁻³⁵

On the 16th day, the tumor tissues were extracted to separate the tumor cells for Western blot assay of apoptosis-related proteins (Figure 6D). Remarkably, in the group of 1-C12G1@DOX/miR-21i polyplexes, the tumor cells display the highest expression levels of BAX, PTEN and p53 proteins among all groups ($p < 0.01$), which is in good consistence with the *in vitro* therapeutic results (Figure 6E-G). These data imply that the synthesized amphiphilic phosphorus dendron micelles are able to encapsulate DOX and condense miR-21i to implement a synergistic tumor therapy effect *in vivo*.

Then, the tumor tissue samples were further examined *via* H&E (Figure S15) and TUNEL (Figure 7) staining. Clearly, tumors treated with the 1-C12G1@DOX/miR-21i polyplexes reveal the highest levels of necrotic and apoptotic cells, validating the excellent therapeutic efficacy of the co-delivery system mediated by the developed 1-C12G1 micelles. This trend was also confirmed by quantification of the cell apoptosis rate based on the population of TUNEL-positive cells in the

tumor sections (Figure S16). The tumor cell apoptosis rate is in an order of 1-C12G1@DOX/miR-21i ($87.3 \pm 3.4\%$) > 1-C12G1@DOX ($78.3 \pm 6.4\%$) > free DOX ($54.2 \pm 2.4\%$) > 1-C12G1/miR-21i ($39.6 \pm 1.4\%$) > 1-C12G1 ($3.0 \pm 0.3\%$) > NS ($1.0 \pm 0.2\%$). These results match the results obtained above using flow cytometry (Figure 3D).

Apparently, the developed 1-C12G1 micelles with a nanoscale size are able to co-deliver both DOX and miR-21i to the tumor region through the passive enhanced permeability and retention (EPR) effect, thereby exerting a synergistic tumor chemo/gene therapeutic efficacy.

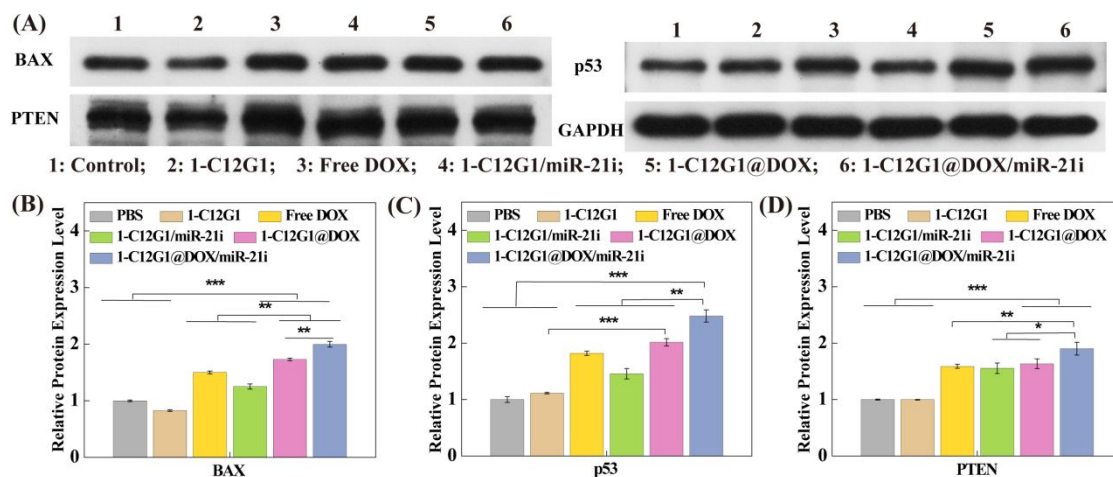


Figure 5. (A) Western Blot assay of the expression of protein relevant to cell apoptosis in MDA-MB-231 cells treated with 1-C12G1, free DOX, 1-C12G1/miR-21i, 1-C12G1@DOX or 1-C12G1@DOX/miR-21i (the equivalent concentration of DOX was $1 \mu\text{M}$). PBS was used as control. Quantification of BAX (B), p53 (C), and PTEN (D) proteins relevant to cell apoptosis from the Western blotting data *in vitro* (* $p < 0.05$, ** $p < 0.01$, and *** $p < 0.005$, respectively).

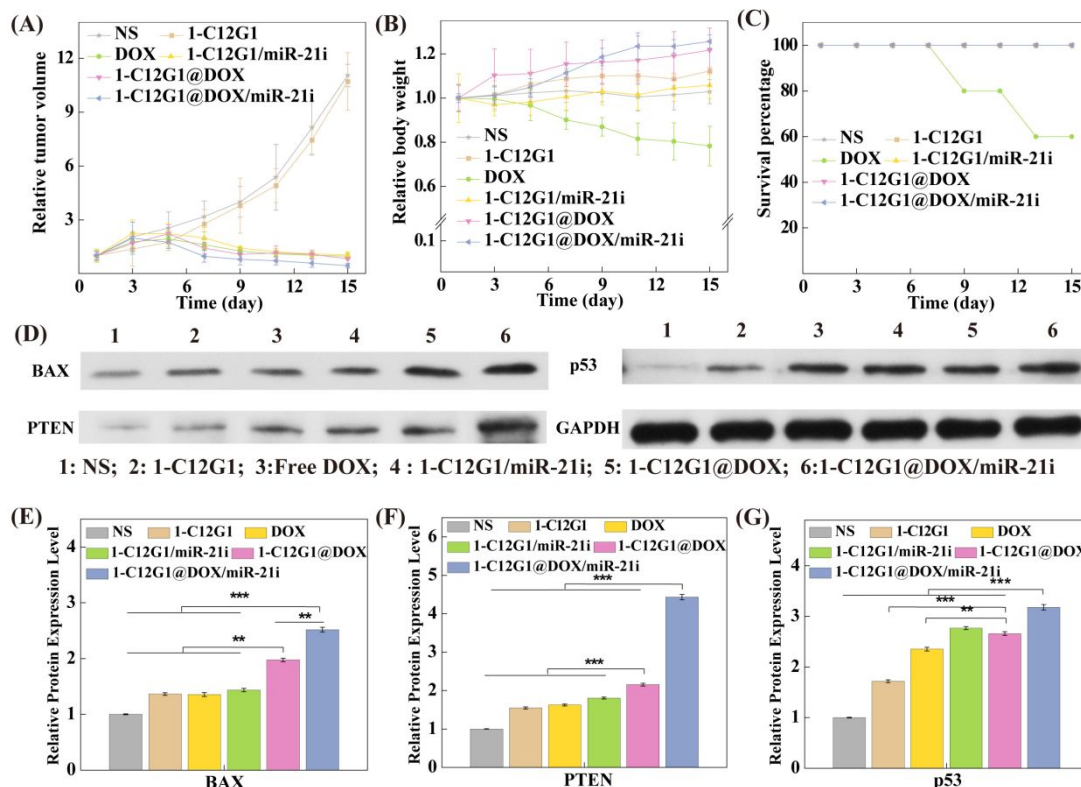


Figure 6. (A) Relative tumor volume measured at given time points after different treatments ($n = 5$ for each group). (B) The relative body weights of mice in different treatment groups versus time post treatments ($n = 5$ for each group). (C) The survival rates of mice measured at given time points after different treatments. (D) Western blot assay of the expression of protein relevant to cell apoptosis in xenografted tumor cells in the treatment groups of 1-C12G1, free DOX, 1-C12G1/miR-21i, 1-C12G1@DOX or 1-C12G1@DOX/miR-21i (the equivalent DOX concentration was $1 \mu\text{M}$). NS was used as control. (C-E) Quantification of the expression levels of cell apoptosis-related proteins of BAX (E), PTEN (F) and p53 (G) in the Western blot data *in vivo* (* $p < 0.05$, ** $p < 0.01$, and *** $p < 0.005$, respectively).

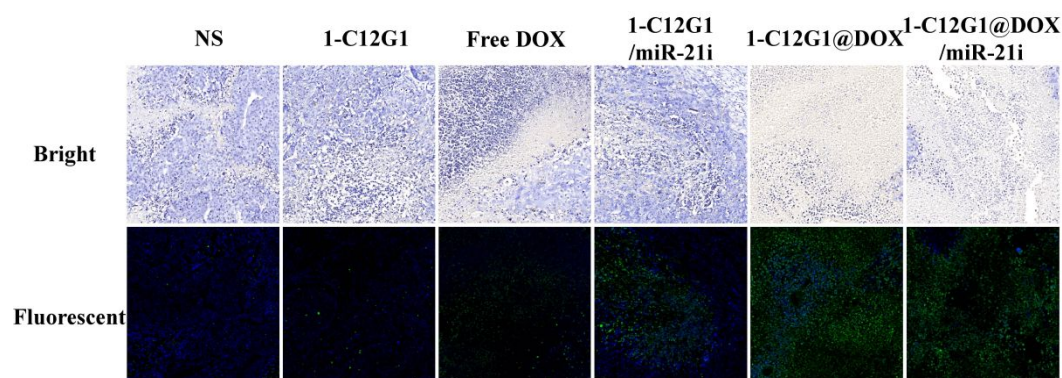


Figure 7. TUNEL staining of the tumor sections from mice treated with NS, 1-C12G1, free DOX, 1-C12G1/miR-21i, 1-C12G1@DOX or 1-C12G1@DOX/miR-21i for 16 days. Scale bar in each panel represents 100 μm .

The histological features of the main organs of mice in different groups were also investigated through H&E staining (Figure 8). Obviously, liver damage can be seen in the free DOX group. To be opposed, no visible organ damage is observed in the groups of 1-C12G1@DOX and 1-C12G1@DOX/miR-21i polyplexes (Figure 8). The significantly alleviated toxicity of 1-C12G1@DOX and 1-C12G1@DOX/miR-21i polyplexes can be ascribed to the micellar

formulation of DOX and miR-21i, which can be accumulated in the tumor site *via* the passive EPR-mediated targeting. Taken together, our results indicate that the developed 1-C12G1@DOX/miR-21i polyplexes can be used to co-deliver both DOX and miR-21i to exert improved tumor inhibition efficacy while reducing the systemic toxicity of DOX *via* rapid drug release at slightly acidic tumoral pH and the passive EPR effect.

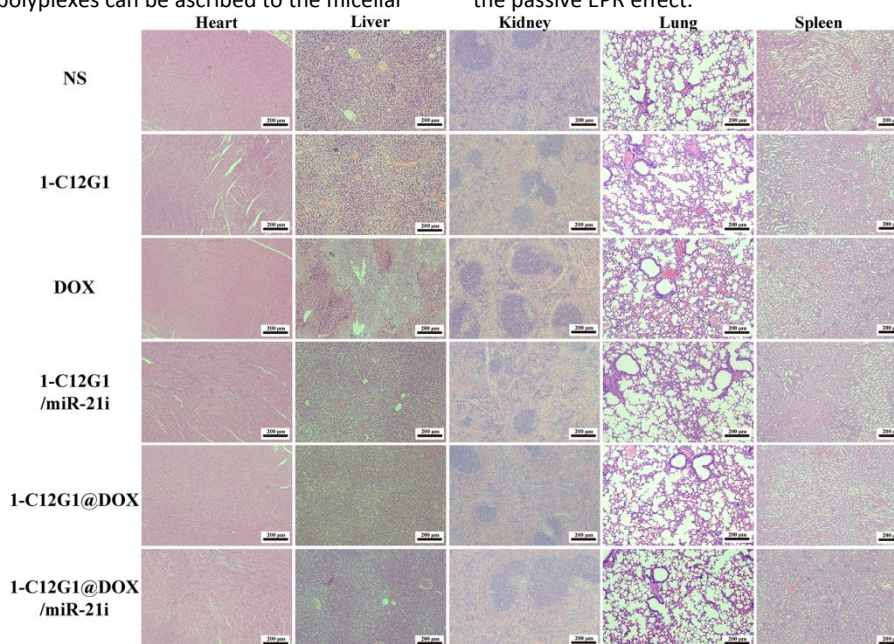


Figure 8. H&E-stained organ sections from mice in the NS, 1-C12G1, free DOX, 1-C12G1/miR-21i, 1-C12G1@DOX or 1-C12G1@DOX/miR-21i treatment group for 16 days. Scale bar in each panel represents 200 μm .

Experimental

Preparation and characterization of amphiphilic phosphorus dendrons

As shown in Figure 1, we prepared an amphiphilic phosphorus dendron bearing a long alkyl chain ($\text{C}_{12}\text{H}_{25}$) directly grafted on the N_3P_3 core and ten protonated pyrrolidine groups on the surface. This amphiphilic phosphorus dendron as well as all the intermediate products were synthesized in good overall yields. The AB_5 monomer

(3) was synthesized through condensation of 4-hydroxybenzaldehyde (2) with hexachlorocyclotriphosphazene (1) (THF, room temperature) to have a 76% yield. Next, by reacting 3 with the amino-phenol-derivative (4) (cesium carbonate, THF, room temperature), the dendron 5 was synthesized in an 80% yield. Further reaction of 5 with (1-methylhydrazinyl) phosphonothioic dichloride (6) (dichloromethane) at room temperature led to the synthesis of 7 (92% yield), which in turn was reacted with 1-(2-aminoethyl) pyrrolidine (8) (cesium carbonate, THF) at room temperature to produce the dendron C12G1NC4 in a 95% yield. Lastly, the pyrrolidine groups of C12G1NC4 were protonated in THF

at room temperature to give the corresponding water-soluble amphiphilic dendrons 1-C12G1 in a 95% yield. Each product was characterized *via* different NMR techniques.

Preparation of 1-C12G1@DOX/miR-21i polyplexes

The 1-C12G1@DOX micelles were formed through incubation of 1-C12G1 and appropriate amount of hydrophobic DOX under different molar ratios (1-C12G1/DOX = 1: 15, 1: 20, 1: 25, 1: 30 and 1: 35, respectively). Each mixture was stirred overnight at room temperature, and centrifuged (7000 rpm for 20 min) to remove the precipitates related to non-encapsulated DOX. The supernatant was then freeze-dried for up to 3 days to acquire the 1-C12G1@DOX complexes. Later, miR-21i and appropriate amount of 1-C12G1@DOX were mixed under various N/P values in diethyl procarbonate (DEPC) water and incubated for 30 min at room temperature to form the 1-C12G1@DOX/miR-21i polyplexes.

Cell culture and *in vitro* anti-proliferative activity

Human triple-negative breast cancer cells (MDA-MB-231 cells) and mouse normal fibroblast cells (NIH-3T3 cells) were regularly cultured in medium supplemented with 10% fetal bovine serum and 1% penicillin-streptomycin. Cells were treated with the 1-C12G1@DOX/miR-21i polyplexes for a certain period of time to examine their cytotoxicity, cellular uptake, and anticancer mechanisms.

Animal experiments

All animal experiments were approved by the ethical committee for animal care of Donghua University and also following the regulations of the National Ministry of Health (China). The tumor-bearing mice were intravenously injected with 0.9% normal saline (NS, Group 1), 1-C12G1 (Group 2), free DOX (Group 3), 1-C12G1/miR-21i (Group 4), 1-C12G1@DOX (Group 5), and 1-C12G1@DOX/miR-21i (Group 6) every 3 days for 5 times, respectively. Each mouse was injected with the dose of 5 mg DOX/kg or 1.2 mg 1-C12G1/kg. We examined the tumor volumes and the body weights every two days. At 16 days post treatment, the mice were sacrificed to extract the tumor tissues and the main organs (heart, liver, spleen, lung, and kidney) for hematoxylin-eosin (H&E) and TdT-mediated dUTP Nick-End Labeling (TUNEL) staining according to standard protocols. For more details, please see the Supporting Information.

Conclusions

We developed amphiphilic phosphorus dendron (1-C12G1) micelles as a platform to co-deliver anticancer drug DOX and miRNA-21i, a genetic tumor suppressive material for synergistic therapy of TNBC. The unique structural features of the dendron micelles having a mean size of 25 nm include hydrophobic interior space and the positive surface potential, making them suitable to effectively load DOX and compress miR-21i. The created 1-C12G1@DOX/miR-21i polyplexes display a pH-sensitive DOX release profile, and can be efficiently taken up by cancer cells to exert their functions from both DOX and miR-21i to efficiently inhibit the growth of cancer cells *in vitro* and an orthotopic TNBC model *in vivo*. Furthermore, the developed dendron micelle-mediated delivery is beneficial to alleviate the free DOX-induced organ damage, thereby significantly

improving the bioavailability of the drug. This newly developed phosphorous dendron-based micellar delivery system may be developed to co-deliver different drug/gene combinations for different synergistic therapy applications.

Conflicts of interest

There are no conflicts to declare.

Acknowledgements

This research has been financially supported by the National Natural Science Foundation of China (81761148028 and 22150410324), the Science and Technology Commission of Shanghai Municipality (21490711500), Shanghai Municipal Health Commission (20214Y0133), China Postdoctoral Science Foundation (2022M712130), and the Shanghai Education Commission through the Shanghai Leading Talents Program. J.P.M, S.M, A.M.C and R.L. thank the collaborative NSFC-CNRS grant (from the France part) for financial support.

Notes and references

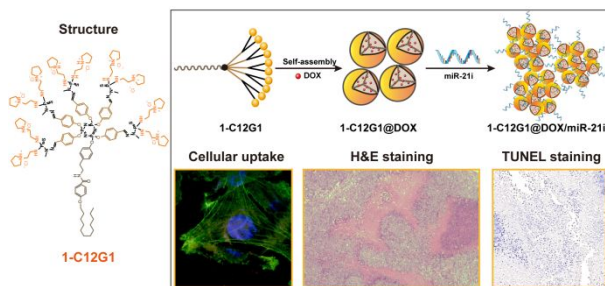
1. R. J. Youle and A. Strasser, *Nat. Rev. Mol. Cell Biol.*, 2008, **9**, 47-59.
2. L. Zhang, Z. Lu, Q. Zhao, J. Huang, H. Shen and Z. Zhang, *Small*, 2011, **7**, 460-464.
3. X. Deng, M. Cao, J. Zhang, K. Hu, Z. Yin, Z. Zhou, X. Xiao, Y. Yang, W. Sheng, Y. Wu and Y. Zeng, *Biomaterials*, 2014, **35**, 4333-4344.
4. D. P. Bartel, *Cell*, 2004, **116**, 281-297.
5. E. Huntzinger and E. Izaurralde, *Nat. Rev. Genet.*, 2011, **12**, 99-110.
6. D. Hanahan and R. A. Weinberg, *Cell*, 2011, **144**, 646-674.
7. A. W. Tong and J. Nemunaitis, *Cancer Gene Ther.*, 2008, **15**, 341-355.
8. L. Lin, Y. Fan, F. Gao, L. Jin, D. Li, W. Sun, F. Li, P. Qin, Q. Shi, X. Shi and L. Du, *Theranostics*, 2018, **8**, 1923-1939.
9. T. J. Lee, J. Y. Yoo, D. Shu, H. Li, J. Zhang, J.-G. Yu, A. C. Jaime-Ramirez, M. Acunzo, G. Romano, R. Cui, H.-L. Sun, Z. Luo, M. Old, B. Kaur, P. Guo and C. M. Croce, *Mol. Ther.*, 2017, **25**, 1544-1555.
10. M. L. Si, S. Zhu, H. Wu, Z. Lu, F. Wu and Y. Y. Mo, *Oncogene*, 2007, **26**, 2799-2803.
11. C. Song, Y. Xiao, Z. Ouyang, M. Shen and X. Shi, *J. Mater. Chem. B*, 2020, **8**, 2768-2774.
12. D. Cheng, N. Cao, J. Chen, X. Yu and X. Shuai, *Biomaterials*, 2012, **33**, 1170-1179.
13. H. Wang, Y. Zhao, Y. Wu, Y.-I. Hu, K. Nan, G. Nie and H. Chen, *Biomaterials*, 2011, **32**, 8281-8290.
14. C.-M. J. Hu, S. Aryal and L. Zhang, *Ther. Delivery*, 2010, **1**, 323-334.
15. M. Creixell and N. A. Peppas, *Nano Today*, 2012, **7**, 367-379.
16. T. Wei, C. Chen, J. Liu, C. Liu, P. Posocco, X. Liu, Q. Cheng, S. Huo, Z. Liang, M. Fermeglia, S. Pricl, X.-J. Liang, P. Rocchi and L. Peng, *Proc. Natl. Acad. Sci. U. S. A.*, 2015, **112**, 2978-2983.
17. H. Cabral, Y. Matsumoto, K. Mizuno, Q. Chen, M. Murakami, M. Kimura, Y. Terada, M. R. Kano, K. Miyazono, M. Uesaka, N. Nishiyama and K. Kataoka, *Nat. Nanotechnol.*, 2011, **6**, 815-823.
18. V. P. Chauhan, T. Stylianopoulos, J. D. Martin, Z. Popovic, O. Chen, W. S. Kamoun, M. G. Bawendi, D. Fukumura and R. K. Jain, *Nat. Nanotechnol.*, 2012, **7**, 383-388.

19. T. Xiao, W. Hou, X. Cao, S. Wen, M. Shen and X. Shi, *Biomater. Sci.*, 2013, **1**, 1172-1180.
20. F. Abedi-Gaballu, G. Dehghan, M. Ghaffari, R. Yekta, S. Abbaspour-Ravasjani, B. Baradaran, J. E. N. Dolatabadi and M. R. Hamblin, *Appl. Mater. Today*, 2018, **12**, 177-190.
21. X. X. Liu, J. H. Zhou, T. Z. Yu, C. Chen, Q. Cheng, K. Sengupta, Y. Y. Huang, H. T. Li, C. Liu, Y. Wang, P. Posocco, M. H. Wang, Q. Cui, S. Giorgio, M. Fermeglia, F. Q. Qu, S. Pricl, Y. H. Shi, Z. C. Liang, P. Rocchi, J. J. Rossi and L. Peng, *Angew. Chem., Int. Ed.*, 2014, **53**, 11822-11827.
22. D. Wang, Y., L. Chen, Y. Gao, C. Song, Z. Ouyang, J., C. Li, S., S. Mignani, J. Majoral, X. Shi, Y, and M. Shen, W,, *J. Mater. Chem. B*, 2021, **9**, 6149-6154.
23. J. Li, L. Chen, C. Li, Y. Fan, M. Zhan, H. Sun, S. Mignani, J.-P. Majoral, M. Shen and X. Shi, *Theranostics*, 2022, **12**, 3407-3419.
24. L. Chen, J. Li, Y. Fan, J. Qiu, L. Cao, R. Laurent, S. Mignani, A.-M. Caminade, J.-p. Majoral and X. Shi, *Biomacromolecules*, 2020, **21**, 2502-2511.
25. V. Percec, D. A. Wilson, P. Leowanawat, C. J. Wilson, A. D. Hughes, M. S. Kaucher, D. A. Hammer, D. H. Levine, A. J. Kim, F. S. Bates, K. P. Davis, T. P. Lodge, M. L. Klein, R. H. DeVane, E. Aqad, B. M. Rosen, A. O. Argintaru, M. J. Sienkowska, K. Rissanen, S. Nummelin and J. Ropponen, *Science*, 2010, **328**, 1009-1014.
26. T. Xiao, X. Cao, W. Hou, C. Peng, J. Qiu and X. Shi, *J. Nanosci. Nanotechnol.*, 2015, **15**, 10134-10140.
27. S. D. Conner and S. L. Schmid, *Nature*, 2003, **422**, 37-44.
28. S. Mura, J. Nicolas and P. Couvreur, *Nat. Mater.*, 2013, **12**, 991-1003.
29. V. P. Torchilin, *Nat. Rev. Drug Discovery*, 2014, **13**, 813-827.
30. G. Li, Y. Fan, L. Lin, R. Wu, M. Shen and X. Shi, *Sci. China Chem.* , 2021, **64**, 817-826.
31. L. Li, L. Yuan, J. Luo, J. Gao, J. Guo and X. Xie, *Clin. Exp. Med.*, 2013, **13**, 109-117.
32. S.-J. Kim, J.-S. Oh, J.-Y. Shin, K.-D. Lee, K. W. Sung, S. J. Nam and K.-H. Chun, *J. Controlled Release*, 2011, **155**, 427-434.
33. S. Raj, V. I. Franco and S. E. Lipshultz, *Curr. Treat. Options Cardiovasc. Med.* , 2014, **16**, 315-315.
34. Y. Octavia, C. G. Tocchetti, K. L. Gabrielson, S. Janssens, H. J. Crijns and A. L. Moens, *J. Mol. Cell. Cardiol.*, 2012, **52**, 1213-1225.
35. E. H. Herman, A. N. Elhage, V. J. Ferrans and B. Ardalan, *Toxicol. Appl. Pharmacol.*, 1985, **78**, 202-214.

Table of Contents (TOC) Image

Amphiphilic phosphorous dendron micelles co-deliver microRNA inhibitor and doxorubicin for augmented triple negative breast cancer therapy

Liang Chen^{a,b,c}, Mengsi Zhan^a, Jin Li^a, Liu Cao^a, Huxiao Sun^a, Régis Laurent^{b,c}, Serge Mignani^{d,e}, Anne-Marie Caminade^{b,c*}, Jean-Pierre Majoral^{b,c*}, Xiangyang Shi^{a,e*}



Amphiphilic phosphorous dendron micelles can be developed to co-deliver microRNA inhibitor and doxorubicin to augment triple negative breast cancer therapy.

Electronic Supplementary Information

Amphiphilic Phosphorous Dendron Micelles Co-deliver MicroRNA Inhibitor and Doxorubicin for Augmented Triple Negative Breast Cancer Therapy†

Liang Chen^{a,b,c}, Mengsi Zhan^a, Jin Li^a, Liu Cao^a, Huxiao Sun^a, Régis Laurent^{b,c}, Serge Mignani^{d,e}, Anne-Marie Caminade^{b,c*}, Jean-Pierre Majoral^{b,c*}, Xiangyang Shi^{a,e*}

^a State Key Laboratory for Modification of Chemical Fibers and Polymer Materials, Shanghai Engineering Research Center of Nano-biomaterials and Regenerative Medicine, College of Biological Science and Medical Engineering, Donghua University, Shanghai 201620, People's Republic of China

^b Laboratoire de Chimie de Coordination du CNRS, 205 Route de Narbonne, BP 44099, 31077 Toulouse CEDEX 4, France

^c Université de Toulouse, UPS, INPT, 31077 Toulouse CEDEX 4, France

^d Université Paris Descartes, PRES Sorbonne Paris Cité, CNRS UMR 860, Laboratoire de Chimie et de Biochimie Pharmacologiques et Toxicologique, 45, rue des Saints Pères, 75006 Paris, France

^e CQM - Centro de Química da Madeira, Universidade da Madeira, Campus da Penteada, 9020-105 Funchal, Portugal

KEYWORDS: cationic phosphorus dendrons; micelles; drug delivery; gene delivery; cancer therapy

* Corresponding author. E-mail: anne-marie.caminade@lcc-toulouse.fr (A. M. Caminade), jean-pierre.majoral@lcc-toulouse.fr (J. P. Majoral), and xshi@dhu.edu.cn (X. Shi)

More Experimental Details

Materials. All reactions were carried out in organic solvents using standard high-vacuum and dry-argon techniques. All chemicals were purchased from Acros, Aldrich, or Fluka. All solvents were freshly dried and distilled according to routine procedures before use. MDA-MB-231 cells (a human triple-negative breast cancer cell line) and NIH-3T3 cells (a mouse embryonic fibroblast cell line) were supplied from Institute of Biochemistry and Cell Biology, the Chinese Academy of Sciences (Shanghai, China). Roswell Park Memorial Institute Medium (RPMI-1640), Dulbecco's Modified Eagle Medium (DMEM) and fetal bovine serum (FBS) were from Gibco (Carlsbad, CA). Penicillin and streptomycin were from Gino Biomedical Technology Co., Ltd. (Hangzhou, China). Cell Counting Kit-8 (CCK-8) was from 7 Sea Biotech Co., Ltd. (Shanghai, China). 4',6-Diamidino-2-phenylindole (DAPI) stain solution and F-Actin Labelling Kit *Green Fluorescence* were from Sangon Biotech (Shanghai, China). Annexin V-FITC (Fluorescein Isothiocyanate)/PI (propidium iodide) Apoptosis Detection Kit and PI Cell Cycle Analysis Kit were acquired from BestBio Biotechnology Co., Ltd. (Shanghai, China). Western blot kit and horse radish peroxidase-labeled Goat Anti-Mouse IgG(H+L) were from Beyotime Biotechnology Co., Ltd. (Shanghai, China). The Bicinchoninic Acid Protein Quantitation Kit was from Shanghai Yeason Biotechnology Co., Ltd. (Shanghai, China). Some antibodies including p53, PTEN, BAX and GAPDH were obtained from Wuhan Servicebio Technology Co., Ltd. (Wuhan, China). Water used in all experiments was purified using a PURIST UV Ultrapure Water System (RephiLe Bioscience, Ltd., Shanghai, China) with a resistivity higher than 18.2 M Ω ·cm.

NMR Characterizations. ^1H , ^{13}C , and ^{31}P NMR spectra were recorded with Bruker AV300, DPX300, or AV400 spectrometers. All ^{13}C NMR and ^{31}P NMR spectra were generally recorded by avoiding the disturbance of $\{^1\text{H}\}$. The signal of the non-deuterated solvent served as internal standard.

Compound 3: This compound was prepared and characterized according to the literature.¹ The solution of hexachlorocyclotriphosphazene (4.52 mmol, 1.57 g, 30 mL tetrahydrofuran (THF)) was added into the mixture of 4-hydroxybenzaldehyde (22.60 mmol, 2.75 g) and cesium carbonate (45.20 mmol, 14.72 g) in 50 mL THF at 0 °C. The reaction mixture was stirred overnight at room temperature. Salts were then removed by centrifugation and the supernatant was concentrated under

reduced pressure. The residue was then purified by silica column chromatography (hexane/ethyl acetate, 8/2 to 6/4, v/v) to afford compound 3 as a colorless oil in a 76% yield. ^1H NMR (400 MHz, CDCl_3): δ = 7.24 (m, 10 H, C2 O-H), 7.82 (m, 10 H, C3 O-H), 9.98 (5H, CHO) ppm. $^{31}\text{P}\{^1\text{H}\}$ NMR (121 MHz, CDCl_3): δ = 5.19 (d, $^2J_{\text{P-P}}=84$ Hz, P_{01} , P_{02}), 20.73 (dd, $^2J_{\text{P-P}}=88$ Hz, $^2J_{\text{P-P}}=84$ Hz, P_{03}) ppm. $^{13}\text{C}\{^1\text{H}\}$ NMR (100 MHz, CDCl_3): δ = 121.40 (m, C2 O), 131.44 (s, C3 O), 133.77 (m, C4 O), 154.29 (m, C1 O), 190.36 (s, CHO), 190.48 (s, CHO) ppm.

Compound 4: To a solution of the tyramine (3.64 mmol) in 5 mL of methanol (MeOH) was added a solution of 4-dodecyloxybenzoic acid (3.64 mmol) and 1-(3-dimethylaminopropyl)-3-ethylcarbodiimide hydrochloride (EDC·HCl, 3.64 mmol) in CHCl_3 (5 mL). This mixture was refluxed overnight. The solution was concentrated under reduced pressure. The resulting product was then purified by silica column chromatography (MeOH/dichloromethane (DCM), 1/19, v/v) to afford compound 4 as a pale yellow powder in an 85% yield. ^1H NMR (400 MHz, DMSO): δ = 0.85 (t, $^3J_{\text{(H-H)}}=8$ Hz, 3 H, Co 'O-H), 1.24 (m, 16 H, Cn 'O-H, Cm 'O-H, Cl 'O-H, Ck 'O-H), 1.40 (m, 2 H, Cj 'O-H), 1.71 (t, $^3J_{\text{(H-H)}}=8$ Hz, 2 H, Ci 'O-H), 2.70 (t, $^3J_{\text{(H-H)}}=6$ Hz, 2 H, Ca 'O-H), 3.39 (m, 2 H, Cb 'O-H), 4.00 (t, $^3J_{\text{(H-H)}}=6$ Hz, 2 H, Ch 'O-H), 6.68 (d, $^3J_{\text{(H-H)}}=8$ Hz, 2 H, C2 'O-H), 6.96 (d, $^3J_{\text{(H-H)}}=8$ Hz, 2 H, C3 'O-H), 7.02 (d, $^3J_{\text{(H-H)}}=12$ Hz, 2 H, Cf 'O-H), 7.79 (d, $^3J_{\text{(H-H)}}=12$ Hz, 2 H, Ce 'O-H), 8.35 (t, $^3J_{\text{(H-H)}}=6$ Hz, 1 H, NH-Cc 'O), 9.16 (s, 1 H, OH) ppm. $^{13}\text{C}\{^1\text{H}\}$ NMR (100 MHz, DMSO): δ = 14.41 (s, Co 'O), 22.56 (s, Cn 'O), 25.92 (s, Cj 'O), 29.05 (s, Cl 'O), 29.34 (m, Ck 'O, Ci 'O), 31.76 (s, Cm 'O), 34.91 (s, Ca 'O), 41.66 (s, Cb 'O), 68.05 (s, Ch 'O), 114.28 (s, Cf 'O), 115.54 (s, C2 'O), 127.15 (s, Cd 'O), 129.32 (s, C3 'O), 129.91 (s, Ce 'O), 130.08 (s, C4 'O), 156.05 (s, C1 'O), 161.31 (s, Cg 'O), 165.99 (s, Cc 'O) ppm.

Compound 5: Compound 4 was added at 0 °C to a solution of cesium carbonate and compound 3 in anhydrous THF (20 mL). The reaction mixture was stirred overnight at room temperature and then centrifuged. The supernatant was then concentrated under reduced pressure. The resulting product was purified by silica column chromatography (pentane/ethyl acetate, 8/2 to 6/4, v/v) to afford compound 5 as a white powder in an 80% yield. ^1H NMR (400 MHz, CDCl_3): δ = 0.89 (t, $^3J_{\text{(H-H)}}=8$ Hz, 3 H, Co 'O-H), 1.27 (m, 16 H, Cn 'O-H, Cm 'O-H, Cl 'O-H and Ck 'O-H), 1.44 (m, 2 H, Cj 'O-H), 1.79 (t, $^3J_{\text{(H-H)}}=8$ Hz, 2 H, Ci 'O-H), 2.91 (t, $^3J_{\text{(H-H)}}=8$ Hz, 2 H, Ca 'O-H), 3.67 (m, 2 H, Cb 'O-H), 3.98 (t, $^3J_{\text{(H-H)}}=8$ Hz, 2 H, Ch 'O-H), 6.22 (t, $^3J_{\text{(H-H)}}=6$ Hz, 1 H, NH-Cc 'O), 6.89 (d, $^3J_{\text{(H-H)}}=8$ Hz, 2 H, Cf 'O-H), 6.94 (d, $^3J_{\text{(H-H)}}=8$ Hz, 2 H, Ce 'O-H), 7.13 (m, 12 H, C2 'O-H and C2 O-H), 7.71 (m, 12 H, C3 'O-H and C3 O-H), 9.94 (s, 5 H, CHO) ppm. $^{31}\text{P}\{^1\text{H}\}$ NMR (162 MHz,

CDCl₃): δ = 7.40 (m, P₀) ppm. ¹³C{¹H} NMR (100 MHz, CDCl₃): δ = 14.12 (s, Co 'O), 22.68 (s, Cn 'O), 25.98 (s, Cj 'O), 29.13 (s, Cl 'O-H), 29.49 (m, Ck 'O and Ci 'O), 31.90 (s, Cm 'O), 35.10 (s, Ca 'O), 40.99 (s, Cb 'O), 68.21 (s, Ch 'O), 77.03 (CDCl₃), 114.24 (s, Cf 'O), 120.74 (br s, C2 'O), 121.25 (s, C2 O), 126.36 (s, Cd 'O), 128.55 (s, C4 O), 129.91 (s, C3 'O), 131.34 (s, C3 O), 133.67 (s, Ce 'O), 136.71 (s, C4 'O), 148.53 (br s, C1 'O), 154.60 (s, C1 O), 161.82(s, Cg 'O), 167.03 (s, Cc 'O), 190.39 (s, CHO), 190.43 (s, CHO), 190.54 (s, CHO) ppm.

Compound 7: A freshly compound 6 (2.1 mmol) synthesized according to the literature² was added at 0 °C to a solution of compound 5 (4.2 mmol) in anhydrous DCM (50 mL). The solution was stirred for 6 h at room temperature and then concentrated under reduced pressure (10 mL). Then, 100 mL of pentane was added to the residue and the resulting precipitate was filtered off and dried under reduced pressure to afford compound 7 as a white powder in a 92% yield. ¹H NMR (400 MHz, CDCl₃): δ = 0.90 (t, ³J_(H-H)=8 Hz, 3 H, Co 'O-H), 1.28 (m, 16 H, Cn 'O-H, Cm 'O-H, Cl 'O-H and Ck 'O-H), 1.46 (m, 2 H, Cj 'O-H), 1.80 (t, ³J_(H-H)= 8 Hz, 2 H, Ci 'O-H), 2.88 (t, ³J_(H-H)= 8 Hz, 2 H, Ca 'O-H), 3.50 (d, ³J_(H-P1)= 16 Hz, 15 H, CH₃-N-P₁), 3.61 (m, 2 H, Cb 'O-H), 3.99 (t, ³J_(H-H)= 8 Hz, 2 H, Ch 'O-H), 6.04 (t, ³J_(H-H)= 6 Hz, 1 H, NH-Cc 'O), 6.92 (m, 4 H, Cf 'O-H and Ce 'O-H), 7.03 (m, 12 H, C2 'O-H and C2 O-H), 7.64 (m, 17 H, C3 'O-H, C3 O-H and CH=N) ppm. ³¹P{¹H} NMR (162 MHz, CDCl₃): δ = 8.36 (m, P₀), 62.41, 62.44 (s, P₁) ppm. ¹³C{¹H} NMR (100 MHz, CDCl₃): δ = 14.13 (s, Co 'O), 22.69 (s, Cn 'O), 26.00 (s, Cj 'O), 29.14 (s, Cl 'O), 29.50 (m, Ck 'O and Cj 'O), 31.89 (s, Cm 'O), 31.97 (d, ²J_(C-P1)= 11 Hz, CH₃-N-P₁), 35.23 (s, Ca 'O), 41.21 (s, Cb 'O), 68.24 (s, Ch 'O), 114.31 (s, Cf 'O), 121.12 (br s, C2 'O), 121.38 (s, C2 O), 126.24 (s, Cd 'O), 128.60 (s, C4 O), 129.76 (s, C3 'O), 131.27 (m, C3 O), 131.16 (s, Ce 'O), 136.02 (s, C4 'O), 140.68 (m, CH=N), 148.77 (br s, C1 'O), 151.66 (s, C1 O), 161.87(s, Cg 'O), 166.95 (s, Cc 'O) ppm.

Compound C12GINC4: To a solution of compound 7 (2.26 mmol) in THF (40 mL) was added at 0 °C compound 8 (22.6 mmol) and N,N-diisopropylethylamine (27.12 mmol). The reaction mixture was stirred overnight at room temperature and then concentrated under reduced pressure. After that, 100 mL of pentane was added to the residue and the resulting precipitate was filtered off and dried under reduced pressure to afford C12GINC4 as a white powder in a 95% yield. ¹H NMR (400 MHz, CDCl₃): δ = 0.89 (t, ³J_(H-H)= 8 Hz, 3 H, Co 'O-H), 1.28 (m, 16 H, Cn 'O-H, Cm 'O-H, Cl 'O-H and Ck 'O-H), 1.45 (m, 2 H, Cj 'O-H), 1.76 (br s, 40 H, C4 1-H), 1.80 (m, 2 H, Ci 'O-H), 2.58 (br s, 40 H, C3 1-H), 2.67 (m, 20 H, C2 1-H), 2.83 (m, 2 H, Ca 'O-H), 3.09 (m, 20 H, C1 1-H), 3.18 (d, ³J_(H-P1)= 8 Hz, 15 H, CH₃-N-P₁), 3.51 (m, 2 H, Cb 'O-H), 3.99 (t, ³J_(H-H)= 8 Hz, 2 H, Ch 'O-H),

4.20 (m, 10 H, NH-P₁), 6.92 (d, ³J_(H-H) = 8 Hz, 2 H, Ce 'O-H), 6.97 (m, 14H, Cf 'O-H, C2 'O-H and C2 O-H), 7.64 (m, 17 H, C3 'O-H, C3 O-H and CH=N) ppm. ³¹P{¹H} NMR (162 MHz, CDCl₃): δ= 8.56 (m, P₀), 68.27, 68.49 (s, P₁) ppm. ¹³C{¹H} NMR (100 MHz, CDCl₃): δ= 14.12 (s, Co 'O), 22.68 (s, Cn 'O), 23.51 (s, C4 1), 26.02 (s, Cj 'O), 29.18 (s, Cl 'O), 29.50 (m, Ck 'O and Cj 'O), 30.90 (d, ²J_(C-P1) = 7 Hz, CH₃-N-P₁), 31.90 (s, Cm 'O), 35.36 (s, Ca 'O), 39.63 (s, C2 1), 41.39 (s, Cb 'O), 53.84 (s, C3 1), 51.23 (d, ²J_(C-P1) = 8 Hz, C1 1), 68.17 (s, Ch 'O), 114.11 (s, Cf 'O), 120.77 (br s, C2 'O), 121.12 (s, C2 0), 126.42 (s, Cd 'O), 127.49 (s, C3 0), 128.91 (s, C4 0), 129.56(s, C3 'O), 132.79 (s, Ce 'O), 132.86 (s, C4 'O), 135.98 (m, CH=N), 150.52 (br s, C1 'O and C1 0), 161.69(s, Cg 'O), 166.90 (s, Cc 'O) ppm.

Critical Micelle Concentration Determination. The critical micelle concentration (CMC) of 1-C12G1 was assessed using pyrene as a fluorescence probe. Water solutions of 1-C12G1 with concentrations ranging from 2.4×10^{-6} to 4.9×10^{-4} M were prepared. Then, each solution was added to a flask containing pyrene at a final concentration of 6.0×10^{-7} M. The solutions were then sonicated for 30 min and kept overnight at room temperature to finalize the micelle formation. Next, the fluorescence spectra were recorded at the excitation wavelength of 333 nm by a fluorescence spectrophotometer (Protein Technologies, Inc., Tucson, MA). Both the excitation and emission bandwidths were set at 5 nm. The pyrene fluorescence intensity ratio of I₃₇₃/I₃₉₃ was analyzed as a function of logarithm 1-C12G1 concentration.

Preparation and Characterization of Doxorubicin (DOX)-Loaded Micelles. Doxorubicin hydrochloride (1.2 to 3.2 mg) was dissolved in 100 μL methanol, and added with triethylamine (molar ratio of DOX/triethylamine = 1: 1) to obtain hydrophobic DOX, which was then mixed with 1-C12G1 (0.5 mg) in 3.0 mL water at different molar ratios (1-C12G1/DOX = 1: 15, 1: 20, 1: 25, 1: 30 or 1: 35). Each mixture solution was stirred overnight at room temperature to allow the evaporation of methanol, and centrifuged (7000 rpm for 10 min) to remove the precipitate related to the non-encapsulated DOX. The precipitate was collected and dissolved into 1 mL methanol for UV-vis spectral analysis using a Lambda 25 UV-vis spectrophotometer (Perkin Elmer, Waltham, MA). The supernatant was lyophilized for 3 days to obtain the 1-C12G1@DOX complex. The drug loading content and drug encapsulation efficiency were calculated according to the following equations:

$$\text{Loading content (\%)} = W_t / W_s \times 100\% \quad (1)$$

$$\text{Encapsulation efficiency (\%)} = W_t / W_0 \times 100\% \quad (2)$$

where W_t represents the mass of loaded DOX within the micelles, W_0 the initial mass of DOX, and W_s the mass of DOX-loaded micelles.

The 1-C12G1@DOX micelles were characterized by fluorescence spectroscopy. Free DOX with the same DOX concentrations was also recorded. The fluorescence emission spectra of the solutions were measured at an excitation wavelength of 365 nm, while the fluorescence excitation spectra of the solutions were collected at an emission wavelength of 595 nm. The micelles before and after DOX loading were also examined using zeta-potential and dynamic light scattering (DLS), which were performed using a Malvern Zetasizer Nano ZS model ZEN3600 (Worcestershire, UK) equipped with a standard 633-nm laser. Transmission electron microscopy (TEM) imaging was executed using the JEOL 2010 analytical electron microscope (JEOL, Tokyo, Japan) at an operating voltage of 200 kV. Each sample was prepared by dropping its aqueous solution onto a carbon-coated copper grid and air dried before measurements.

Preparation and Characterization of 1-C12G1@DOX/miR-21i Polyplexes. The 1-C12G1@DOX/miR-21i (microRNA-21 inhibitor) polyplexes were formed by incubating 1 μ g miR-21i and appropriate amount of 1-C12G1@DOX under different N/P ratios in diethyl procarbonate (DEPC) water, and incubated for 30 min at room temperature. The final volume of the polyplexes was 20 μ L for gel retardation assay. The gel was prepared by dissolving 1% (w/v) agarose gel and 4S Green Plus Nucleic Acid Stain in Tris-acetate-EDTA buffer, and melted using a microwave. Then, the 1-C12G1@DOX/miR-21i polyplexes with different N/P ratios were loaded into the respective wells of the gel, and electrophoresis was carried out at 85 V for 30 min. The retardation of the miR-21i was visualized using a UV transilluminator (Shanghai FURI Science & Technology, Shanghai, China).

For hydrodynamic size and zeta-potential measurements, the 1-C12G1@DOX micelles were dispersed in DEPC water, and then complexed with miR-21i under different N/P ratios. In this case, 5 μ g of miR-21i dissolved in DEPC water was complexed with the 1-C12G1@DOX to reach a final volume of 1 mL. After incubation for 30 min, the prepared polyplexes were subjected to DLS and zeta potential measurements. All measurements were performed at room temperature.

Drug Release Kinetics. The DOX release from the 1-C12G1@DOX/miR-21i polyplex was determined by dialysis using a membrane with a molecular weight cut-off (MWCO) of 8,000-12,000. In brief, 200 μ L of the 1-C12G1@DOX/miR-21i polyplex (1 mg/mL) was dialyzed against phosphate buffer at two different pHs (pH 7.4 and pH 5.0) at 37 $^{\circ}$ C according to the literature.³ At a

predetermined time interval, 1 mL of aliquot of the outer phase medium was withdrawn, and replenished with 1 mL of fresh corresponding medium. The DOX concentration was determined by UV-vis spectrophotometer to calculate the accumulative release of DOX from the 1-C12G1@DOX/miR-21i polyplex.

Cell Culture. NIH-3T3 and MDA-MB-231 cells were regularly cultured and passaged using DMEM and RPMI-1640 medium with 10% FBS and 1% penicillin-streptomycin, respectively. The cells were incubated at 37 °C in a Thermo Scientific cell incubator (Waltham, MA) with 5% CO₂.

Cytotoxicity Assay. The cytotoxicity of 1-C12G1, free DOX, 1-C12G1/miR-21i, 1-C12G1@DOX or 1-C12G1@DOX/miR-21i was quantitatively evaluated by CCK-8 cell viability assay. Cells were cultured in a 96-well plate at a density of 1×10^4 cells per well in 100 μ L medium overnight to bring the cell adherence to the well. Then, the medium of each well was discarded and added with fresh medium containing different materials with varying concentrations. After 24 h, the medium in each well was replaced with 100 μ L serum-free medium containing 10% CCK-8 solution and then the cells were incubated for another 2 h under regular cell culture conditions. After that, the cells in each well were analyzed using a Thermo Scientific Multiskan MK3 ELISA reader (Thermo Scientific, Waltham, MA) at a wavelength of 450 nm. Each sample was tested in sextuplicate.

Cellular Uptake Assay. Cellular uptake of free DOX, 1-C12G1@DOX or 1-C12G1@DOX/miR-21i was investigated by qualitative confocal/fluorescence microscopic imaging and quantitative flow cytometry analysis. For confocal microscopic imaging, MDA-MB-231 cells were seeded into 35-mm confocal dishes (1.5×10^5 cells per dish, 1 mL medium), incubated at 37 °C overnight, and then treated with medium containing free DOX, 1-C12G1@DOX or 1-C12G1@DOX/miR-21i at the equivalent DOX concentration of 1 μ M for 4 h. Cells were then washed with phosphate buffered saline (PBS), stained with F-Actin Labeling Kit *Green Fluorescence* for 30 min, washed with PBS, and stained with DAPI for 5 min. Then, the cells were observed by ZEISS laser scanning confocal microscope (LSM-700, Jena, Germany) at an excitation wavelength of 488 nm. For fluorescence microscopic imaging, cells were seeded into 24-well plates at a density of 1×10^5 cells per well, then treated with the polyplexes as described above. The cells were observed by an Axio Vert.A1 Carl Zeiss fluorescence microscope (Jena, Germany) to validate the DOX uptake. For flow cytometry assay, cells were seeded into 6-well plates at a density of 3×10^5 cells per well, then treated with free DOX, 1-C12G1@DOX or 1-C12G1@DOX/miR-21i as

described above. Cells were then harvested, treated with Trypsin-EDTA, and analyzed using a Becton Dickinson FacsScan analyzer (Franklin Lakes, NJ).

Cell Apoptosis Assay. Annexin V-FITC/PI apoptosis detection kit was used for cell apoptosis assessments. In brief, 3×10^5 MDA-MB-231 cells per well were seeded into 6-well plates, then incubated with 1-C12G1, free DOX, 1-C12G1/miR-21i, 1-C12G1@DOX or 1-C12G1@DOX/miR-21i at the equivalent DOX (or 1-C12G1) concentration ($[DOX] = 1 \mu\text{M}$, or $[1\text{-C12G1}] = 0.04 \mu\text{M}$) for 4 h. Then, cells were washed with PBS, and the medium was replaced with fresh medium containing 10% FBS and 1% penicillin-streptomycin. After 24 h, cells were harvested and processed using Annexin V-FITC/PI apoptosis detection kit in compliance with the manufacturer's protocol, and measured by a Becton Dickinson FacsScan analyzer. Each sample was measured in triplicate.

Western Blot Assay *in Vitro*. To elucidate the molecular mechanism of the cell apoptosis, the cell apoptosis-related proteins were inspected *via* Western blotting *in vitro*. MDA-MB-231 cells were treated as described above, and then exposed to cell lysate buffer to extract proteins. The lysates were centrifuged at 12,000 rpm for 5 min at 4 °C. Thereafter, the supernatants were collected for Western blot assay according to the manufacturer's instructions. Protein concentration was determined with a commercial Bradford Protein Assay Kit. The whole cell protein lysates were electrophoresed on 10% SDS-PAGE (sodium dodecyl sulfate-polyacrylamide gel electrophoresis) and transferred onto polyvinylidene difluoride (PVDF) membranes (Millipore, Bedford, MA), followed by blocking in Tris-buffered saline with 5% non-fat milk, and then incubated with primary antibodies (Cell Signaling Technology, Beverly, MA) at 4 °C overnight. Membranes were then incubated with secondary antibody for 2 h at room temperature. The membranes were detected with an enhanced chemiluminescent reagent (Merck Millipore, Burlington, MA) and exposed to Kodak X-Omat films (Kodak, Xiamen, China). Finally, the films were developed and the intensity of immunoreactivity was measured by densitometry using Image J 1.40 G software (<http://rsb.info.nih.gov/ij/download.html>).

***In Vivo* Antitumor Activity Using an Orthotopic TNBC Tumor Model.** All animal experiments were carried out after approval by the ethical committee for animal care of Donghua University and also in accordance with the policy of the National Ministry of Health (China). To build up an orthotopic triple negative breast cancer (TNBC) tumor model, each BALB/c nude mouse (4-weeks-old, Shanghai Laboratory Animal Center, Shanghai, China) was injected in the right axilla

with 5×10^6 MDA-MB-231 cells suspended in 100 μL of 0.9% normal saline (NS). At about 2 weeks post-injection, the tumor reached about a volume of 100 mm^3 . To investigate the antitumor activity *in vivo*, the tumor-bearing nude mice were divided into 6 groups, and the mice were intravenously injected with NS (Group 1), 1-C12G1 (Group 2), free DOX (Group 3), 1-C12G1/miR-21i (Group 4), 1-C12G1@DOX (Group 5), and 1-C12G1@DOX/miR-21i (Group 6), respectively every 3 days for 5 times. The dose of 5 mg DOX/kg or 1.2 mg 1-C12G1/kg was used for each mouse. The tumor volumes and body weights were recorded every two days. The tumor volume (V) was calculated according to a formula of $V = W^2 \times L/2$, where W and L represent the width and length of tumor, respectively. The relative tumor volume and body weight was calculated based on the tumor volume on the first day. On the 16th day, the main organs (heart, liver, spleen, lung, and kidney) and the tumor tissues were removed from sacrificed mice for hematoxylin-eosin (H&E) and TdT-mediated dUTP Nick-End Labeling (TUNEL) staining according to standard protocols. The TUNEL staining images were also applied to detect the apoptosis rate of tumor cells in different treatment groups. Western blot assay was also applied to detect the relative expression level of apoptosis-related proteins in tumor cells.

Statistical Analysis. Data were presented as the mean \pm standard deviation ($n \geq 3$). One-way analysis of variance statistical method was adopted to analyze the experimental results. A p value of 0.05 was selected as the significance level, and the data were marked with (*) for $p < 0.05$, (**) for $p < 0.01$, and (***) for $p < 0.001$, respectively.

Table S1. Polydispersity index (PDI) of 1-C12G1, 1-C12G1@DOX and 1-C12G1@DOX/miR-21i.

Samples	Low concentration (30.2 μM)	High concentration (151 μM)
1-C12G1	0.314	0.798
1-C12G1@DOX	0.290	0.286
1-C12G1@DOX/miR-21i	0.355	0.144

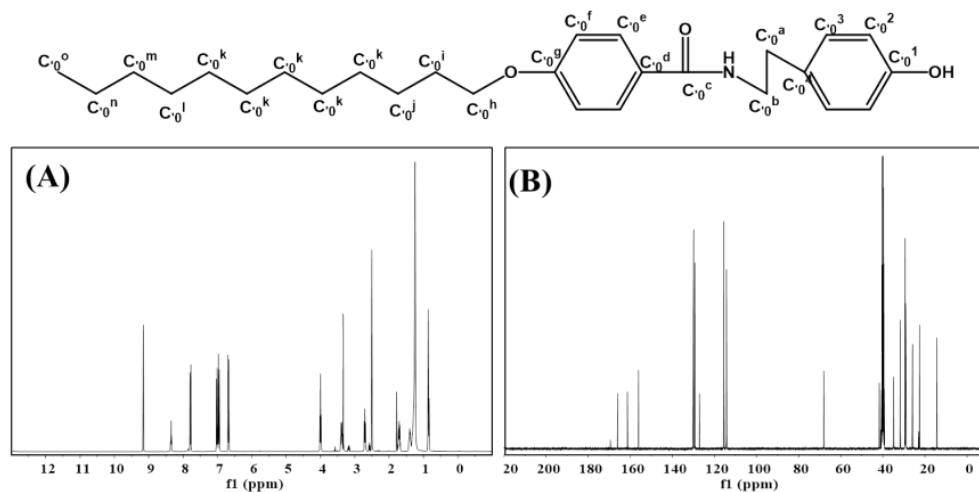


Figure S1. ^1H NMR (A) and $^{13}\text{C}\{^1\text{H}\}$ NMR (B) spectra of compound 4.

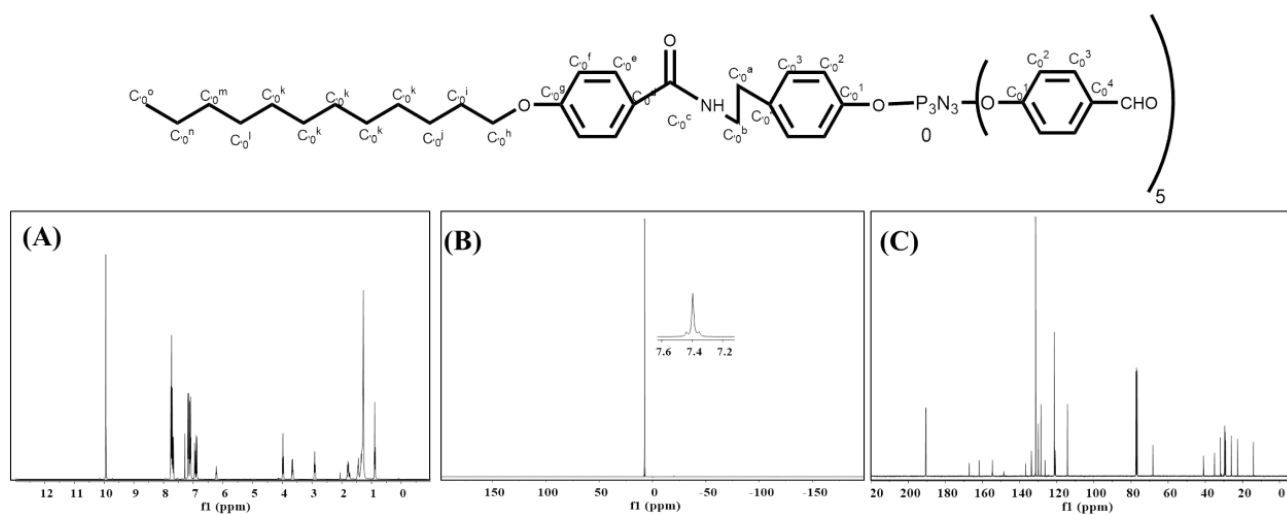


Figure S2. ^1H NMR (A), $^{31}\text{P}\{^1\text{H}\}$ NMR (B) and $^{13}\text{C}\{^1\text{H}\}$ NMR (C) spectra of compound 5.

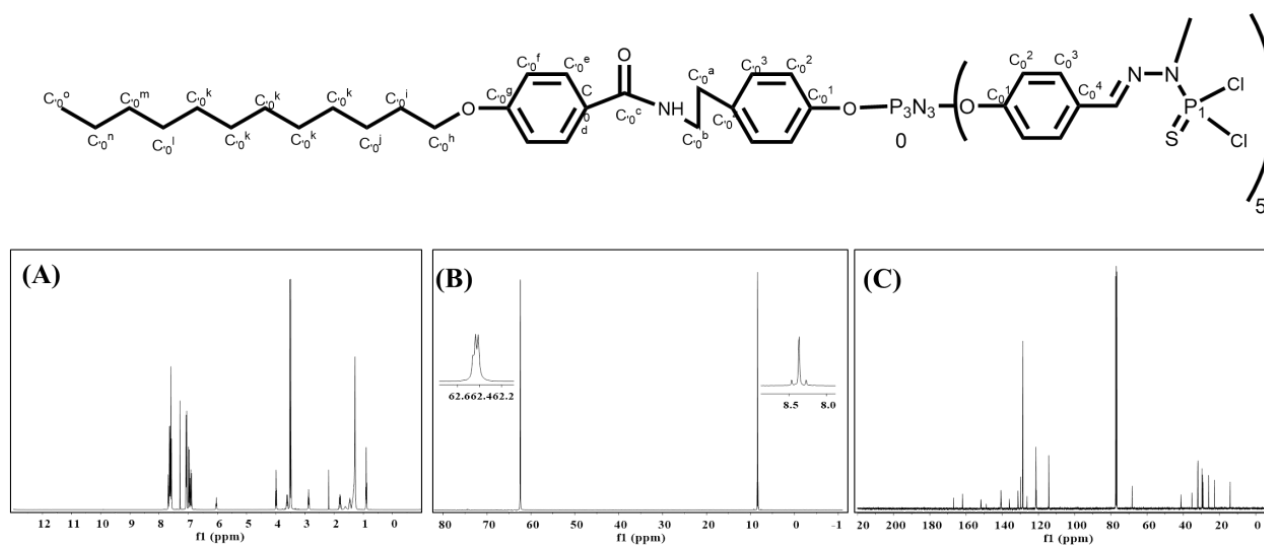


Figure S3. ^1H NMR (A), $^{31}\text{P}\{^1\text{H}\}$ NMR (B) and $^{13}\text{C}\{^1\text{H}\}$ NMR (C) spectra of compound 7.

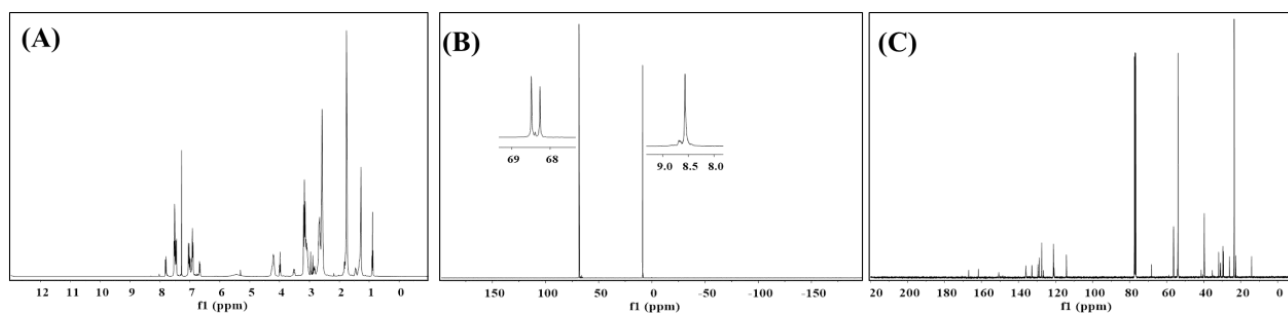
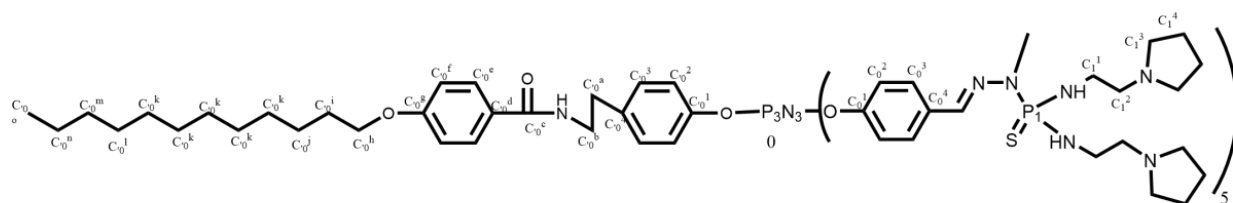


Figure S4. ^1H NMR (A), $^{31}\text{P}\{^1\text{H}\}$ NMR (B) and $^{13}\text{C}\{^1\text{H}\}$ NMR (C) spectra of C12G1NC4.

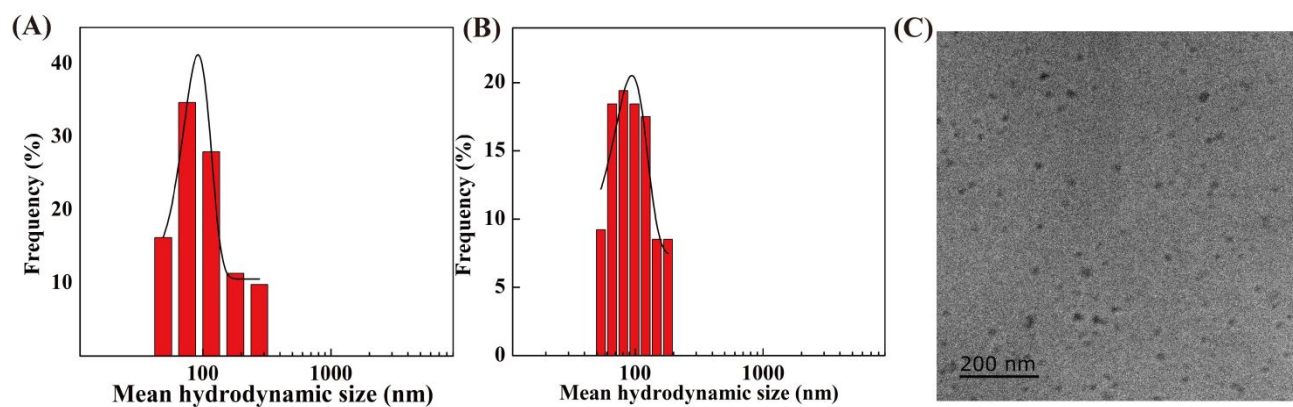


Figure S5. Hydrodynamic size distribution of 1-C12G1 micelles dispersed in water at a concentration of (A) 300 μM and (B) 30 μM . (C) TEM image of 1-C12G1 micelles at the dendron concentration of 300 μM .

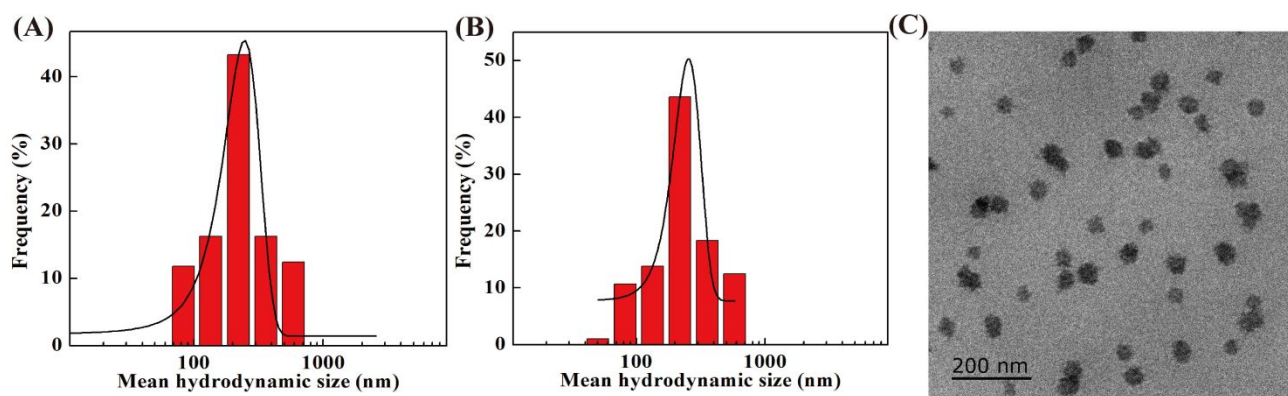


Figure S6. Hydrodynamic size distribution of 1-C12G1@DOX micelles dispersed in water at the equivalent DOX concentration of (A) 79.6 μM and (B) 7.96 μM . (C) TEM image of 1-C12G1@DOX micelles at the equivalent DOX concentration of 79.6 μM .

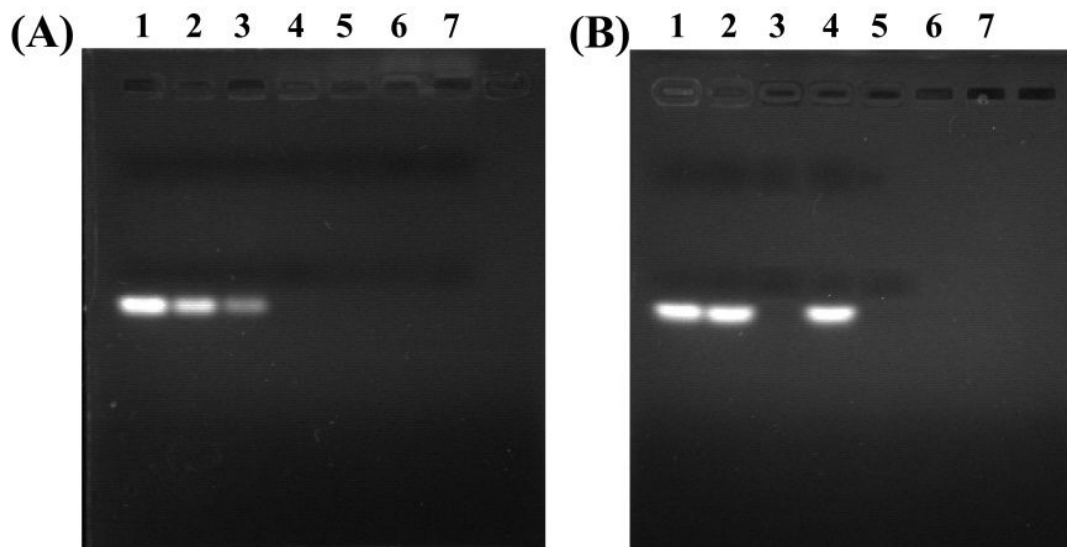


Figure S7. (A) Gel retardation assay of miR-21i complexed with 1-C12G1@DOX at various N/P ratios. Lane 1: miR-21, lane 2: N/P = 0.25: 1, lane 3: N/P = 0.5:1, lane 4: N/P = 1: 1, lane 5: N/P = 2: 1, lane 6: N/P = 3:1, and lane 7: N/P = 4: 1. (B) The stability assessment of free miR-21i and miR-21i complexed with the micelles monitored under normal saline at 37 °C (Lane 1: free miR-21i for 0 h, lane 2: 1-C12G1@DOX/miR-21i for 12 h, lane 3: free miR-21i for 12 h, and lane 4: 1-C12G1@DOX/miR-21i for 24 h, and lane 5: free miR-21i for 24 h).

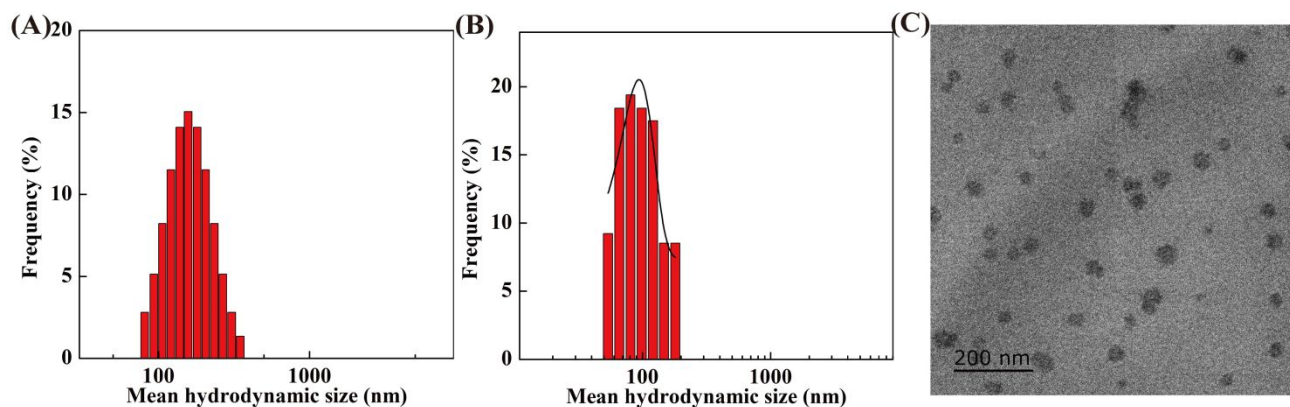


Figure S8. Hydrodynamic size distribution of 1-C12G1@DOX/miR-21i dispersed in water at the equivalent DOX concentration of (A) 79.6 μM and (B) 7.96 μM . (C) TEM image of 1-C12G1@DOX/miR-21i micelles at the equivalent DOX concentration of 79.6 μM .

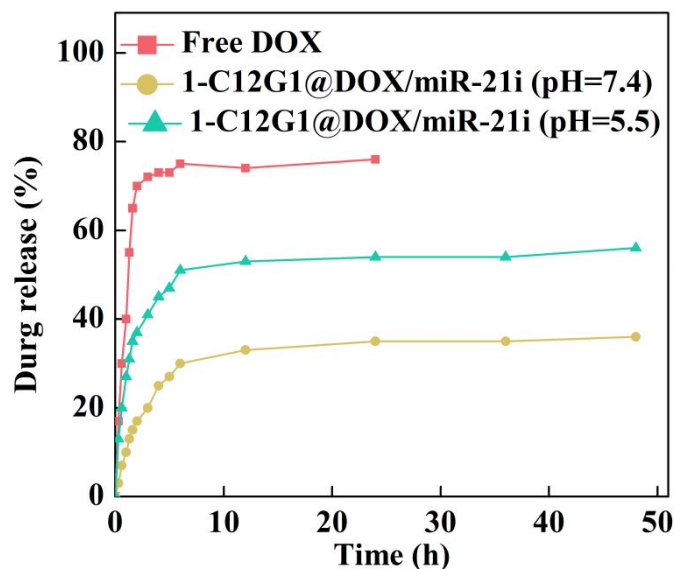


Figure S9. *In vitro* DOX release from 1-C12G1@DOX/miR-21i micelles in phosphate buffer at pH 5.5 or pH 7.4 at 37 °C. Free DOX was also tested for comparison.

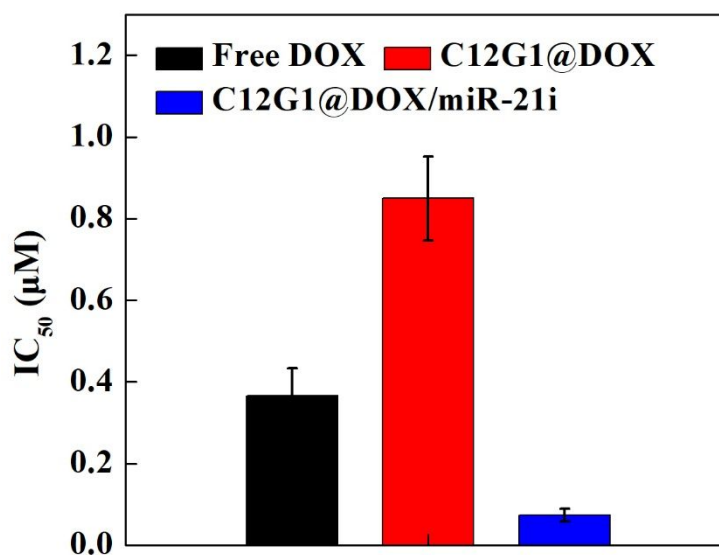


Figure S10. IC₅₀s of free DOX and complexes. Data are shown as the mean of triplicate measurements with standard deviation (n = 3).

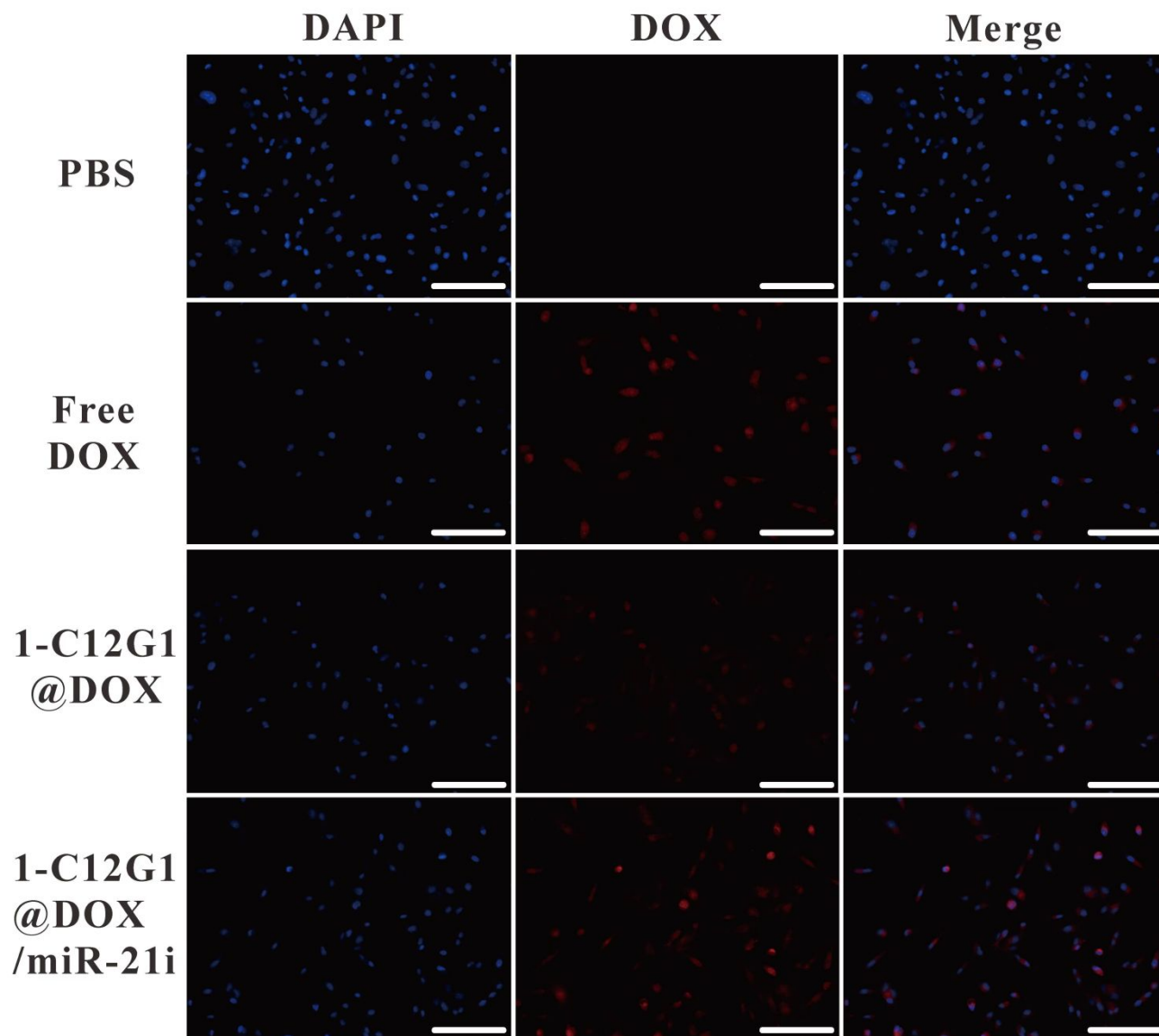


Figure S11. Fluorescence microscopic images of MDA-MB-231 cells treated with free DOX, 1-C12G1@DOX or 1-C12G1@DOX/miR-21i for 4 h (the equivalent concentration of DOX was 1 μ M). Scale bar in each panel represents 100 μ m.

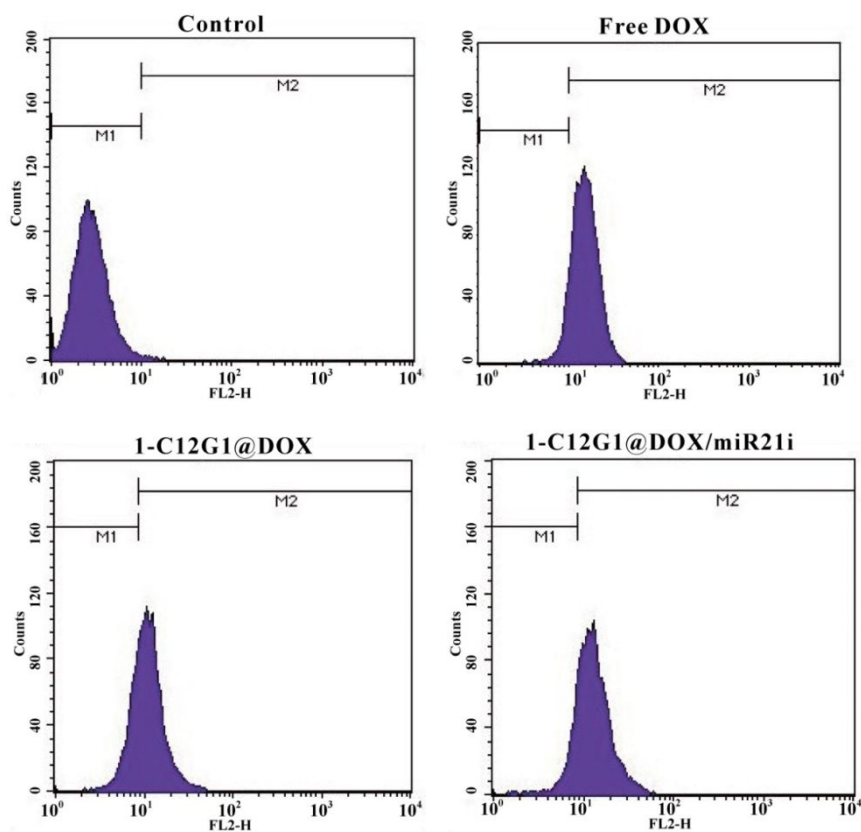


Figure S12. Flow cytometry analysis of MDA-MB-231 cells after treatment with free DOX, 1-C12G1@DOX or 1-C12G1@DOX/miR-21i for 4 h (the equivalent concentration of DOX was 1 μ M).

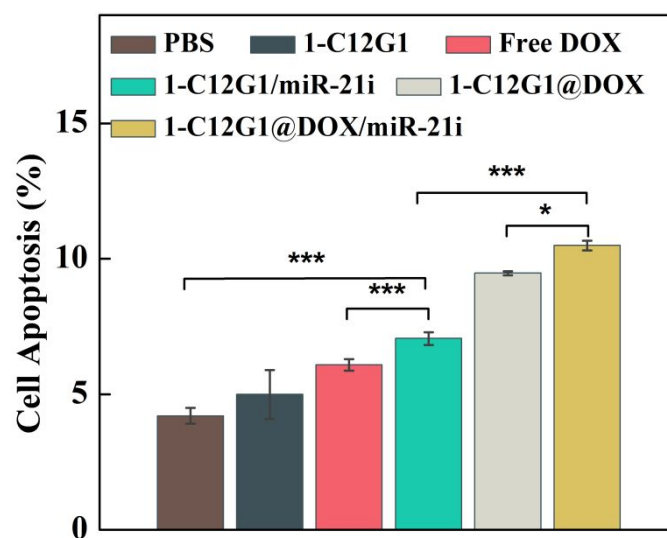


Figure S13. Percentages of apoptotic MDA-MB-231 cells treated with 1-C12G1, free DOX, 1-C12G1/miR-21i, 1-C12G1@DOX or 1-C12G1@DOX/miR-21i (the equivalent concentration of DOX was 1 μ M) analyzed by flow cytometry using annexin V-FITC/PI kit.



Figure S14. Representative photographs of tumor tissues in NS, 1-C12G1, free DOX, 1-C12G1/miR-21i, 1-C12G1@DOX and 1-C12G1@DOX/miR-21i groups on the 16th day.

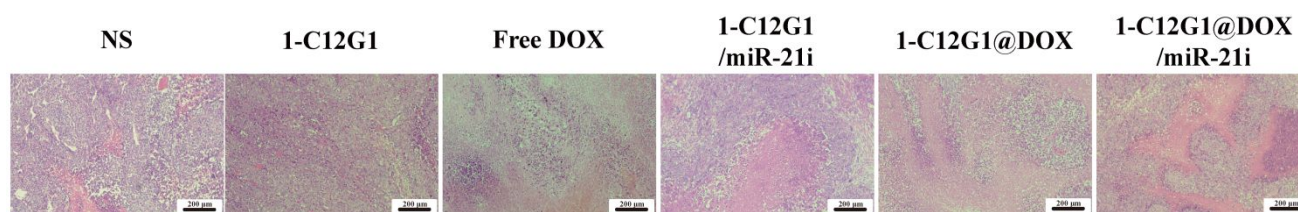


Figure S15. H&E-stained xenografted tumor sections from mice injected with NS, 1-C12G1, free DOX, 1-C12G1/miR-21i, 1-C12G1@DOX or 1-C12G1@DOX/miR-21i at 16 days post-injection. Scale bar in each panel represents 200 μm .

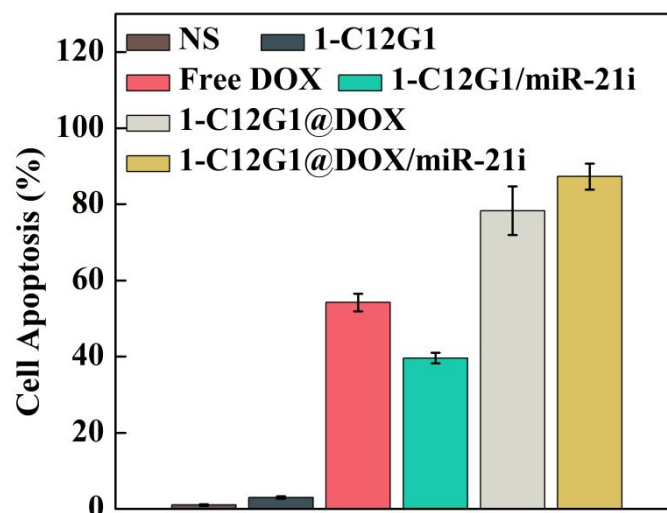


Figure S16. Apoptosis rates of tumor cells after different treatments by quantification of the TUNEL-positive tumor cells in tumor sections.

References

1. G. Franc, S. Mazères, C.-O. Turrin, L. Vendier, C. Duhayon, A.-M. Caminade and J.-P. Majoral, *J. Org. Chem.*, 2007, **72**, 8707-8715.
2. L. Chen, L. Cao, M. Zhan, J. Li, D. Y. Wang, R. Laurent, S. Mignani, A.-M. Caminade, J.-P. Majoral and X. Y. Shi, *Biomacromolecules*, 2022, **23**, 2827-2837.
3. C. Song, Y. Xiao, Z. Ouyang, M. Shen and X. Shi, *J. Mater. Chem. B*, 2020, **8**, 2768-2774.